Bioactive Materials 45 (2025) 567–583

Contents lists available at ScienceDirect

Bioactive Materials

journal homepage: www.keaipublishing.com/en/journals/bioactive-materials

TClC effectively suppresses the growth and metastasis of NSCLC via polypharmacology

Jing Lu [a,1], Ying Zhang [a,b,c,1], Chunyan Yan [a,m,1], Jingwen Liu [d,1], Dan Qi [e,s,1], Yue Zhou [f], Qinwen Wang [g,h], Juechen Yang [i,j], Jing Jiang [k,l], Benhao Wu [b], Meiling Yang [a,b], Weiwei Zhang [a,b], Xin Zhang [a,b], Xiaoyu Shi [a,b], Yan Zhang [a,b], Kun Liu [a], Yongcai Liang [a], Chaoyang Wang [n], Hanyu Yang [o], Yuqing Gao [o], Yuping Sun [p], Ronghu Ke [e], Jason H. Huang [e,q,s], Min Wu [t,u], Hongbo Wang [a], Chunlei Li [o,*****], Shuang Zhou [d,****], Bin Guo [d,***], Erxi Wu [e,q,r,s,v,**], Guoying Zhang [a,*]

[a] School of Pharmacy, Key Laboratory of Molecular Pharmacology and Drug Evaluation (Yantai University), Ministry of Education, Collaborative Innovation Center of Advanced Drug Delivery System and Biotech Drugs in Universities of Shandong, Yantai University, Yantai, Shandong, 264005, China
[b] Shandong Yingdong Yinghao Biotechnology Inc., Yantai, Shandong, 264670, China
[c] Department of Pharmaceutical Sciences, North Dakota State University, Fargo, ND, 58105, USA
[d] Department of Pharmacological & Pharmaceutical Sciences, University of Houston, Houston, TX, 77204, USA
[e] Neuroscience Institute and Department of Neurosurgery, Baylor Scott & White Health, Temple, TX, 76502, USA
[f] Department of Statistics, North Dakota State University, Fargo, ND, 58102, USA
[g] The Center of Non-Traumatic Treatment and Diagnosis of Tumor, Binzhou Medical College affiliated The PLA 107 Hospital, Yantai, Shandong, 264002, China
[h] Outpatient Department, No. 26 Rest Center for Retired Cadres, Haidian district, Beijing, 100036, China
[i] Department of Biomedical Informatics, University of Cincinnati College of Medicine, Cincinnati, OH, USA
[j] Division of Biomedical Informatics, Cincinnati Children's Hospital Medical Center, Cincinnati, OH, USA
[k] RemeGen, Ltd, Yantai, 264000, Shandong, China
[l] Department of Pharmacology, Binzhou Medical University, Yantai, 264003, Shandong, China
[m] Department of Pharmacy, Yantai Yuhuangding Hospital, Yantai, Shandong, 264000, China
[n] Department of Thoracic Surgery, Yantai Yuhuangding Hospital, Yantai, Shandong, 264000, China
[o] Shiyao Zhongqi Pharmaceutical Technology (Shijiazhuang) Co., LTD., State Key Laboratory of New Pharmaceutical Preparations and Excipients, Shijiazhuang, 050035, China
[p] Phase I Clinical Trial Center, Shandong Cancer Hospital and Institute, Shandong First Medical University and Shandong Academy of Medical Sciences, Jinan, Shandong, 250013, China
[q] College of Medicine, Texas A&M University, College Station, TX, 77843, USA
[r] College of Irma Lerma Rangel College of Pharmacy, Texas A&M University, College Station, TX, 77843, USA
[s] Department of Neurosurgery, Baylor College of Medicine, Temple, TX, 76502, USA
[t] Drug Discovery Center, Wenzhou Institute University of Chinese Academy of Sciences, Wenzhou, 325001, China
[u] Department of Critical Care Medicine, Frontiers Science Center for Disease-related Molecular Network, State Key Laboratory of Biotherapy and Cancer Center, West China Hospital, Sichuan University, Chengdu, 646000, China
[v] LIVESTRONG Cancer Institutes and Department of Oncology, Dell Medical School, the University of Texas at Austin, Austin, TX, 78712, USA

ARTICLE INFO

Keywords:
Non-small cell lung cancer
Metastasis

ABSTRACT

Despite significant advances in targeted therapies and immunotherapies, non-small cell lung cancer (NSCLC) continues to present a global health challenge, with a modest five-year survival rate of 28 %, largely due to the emergence of treatment-resistant and metastatic tumors. In response, we synthesized a novel bioactive

* Corresponding author.
** Corresponding author. Neuroscience Institute and Department of Neurosurgery, Baylor Scott & White Health, Temple, TX, 76502, USA.
*** Corresponding author.
**** Corresponding author.
***** Corresponding author.
E-mail addresses: lc884952@163.com (C. Li), goldenshuang1929@gmail.com (S. Zhou), bguo@central.uh.edu (B. Guo), Erxi.Wu@BSWHealth.org (E. Wu), zhang_zhang6173@aliyun.com (G. Zhang).
[1] Equal first authors.

https://doi.org/10.1016/j.bioactmat.2024.11.019
Received 29 June 2024; Received in revised form 10 November 2024; Accepted 15 November 2024

Tea derivative
Polypharmacological effect
Cancer stem cell markers

compound, ethyl 6-chlorocoumarin-3-carboxylyl L-theanine (TClC), which significantly inhibited NSCLC growth, epithelial mesenchymal transition (EMT), migration, and invasion *in vitro* and tumor growth and metastasis *in vivo* without inducing toxicity. TClC disrupts autocrine loops that promote tumor progression, particularly in stem-like CD133-positive NSCLC (CD133+ LC) cells, which are pivotal in tumor metastasis. Through targeted molecular assays, we identified direct binding targets of TClC, including Akt, NF-κB, β-catenin, EZH2, and PD-L1. This interaction not only suppresses the expression of oncogenic factors and cancer stem cell markers but also downregulates the expression of a multidrug resistance transporter, underscoring the compound's polypharmacological potential. These results position TClC as a promising candidate for NSCLC treatment, signaling a new era in the development of cancer therapies that directly target multiple critical cancer pathways.

1. Introduction

According to the 2024 reported data from GLOBOCAN, lung cancer resulted in nearly 2.5 million new cases and over 1.8 million deaths globally in 2022, making it the leading cause of cancer morbidity and mortality [1]. It accounts for 12.4 % of cancer diagnoses and 18.7 % of cancer deaths worldwide [1]. In 2024 alone, there are 234,580 estimated new cases in the United States [2,3]. Non-small cell lung cancer (NSCLC) is the most common type of lung cancer and accounts for 80 %–85 % of all lung cancer cases [2,4,5]. Despite significant advancements in targeted therapies and immunotherapies [6], the five-year survival rate for NSCLC remains at approximately 28 % across all stages [7,8]. The majority of NSCLC patients are diagnosed at an advanced stage, and even those diagnosed early often develop metastatic disease [9]. The 5-year survival rate for advanced and distantly metastatic NSCLC patients is alarmingly low at 9 % [7]. This underscores the urgent need for research into novel drug development strategies and new therapies to improve outcomes for a broader range of patients.

The high mortality and poor clinical outcomes of NSCLC are attributed primarily to therapeutic resistance, cancer progression, and metastasis [5,10–12]. Stem-like cancer cells play crucial roles in drug resistance, tumor relapse, and metastasis, posing significant challenges in lung cancer treatment [13,14]. CD133, an early identified stem cell marker, is linked to cancer stem cells in various tumors, including NSCLC [15,16]. Other markers, such as ALDH1, CD44, ABCG2, and Lgr5, are also highly expressed in stem-like cancer cells across different cancer types, including breast, lung, brain, and colon cancers [17,18]. Cisplatin has been shown to enrich CD133-positive (CD133+) NSCLC cells, which are associated with drug resistance [19]. CD133 also stabilizes or stimulates AKT signaling and interacts with VEGF, enhancing angiogenesis [16,20]. Spatial analysis of NSCLC tumor tissues revealed a high enrichment of CD133+ cells in recurrent patients [21]. However, our understanding of how these cancer cells maintain their stemness, especially in NSCLC, remains incomplete. Further research is crucial to better understand the role of these stem-like tumor cells in NSCLC, particularly regarding disease progression and metastasis. This knowledge is vital for developing new drugs, creating more effective treatments, and improving patient survival rates.

Standard-of-care therapies for NSCLC patients include systemic treatments such as resection, chemotherapy (e.g., cisplatin), targeted therapy (e.g., gefitinib), and immunotherapy [6,22–26]. In advanced stages with widespread tumor presence, genetic testing is conducted to identify specific mutations (e.g., *EGFR, KRAS, ROS1, or BRAF*) to determine potential targeted therapy options, such as the use of gefitinib as an EGFR inhibitor. Antiangiogenic therapy with VEGF/VEGF receptor inhibitors and blockade of the PD-1/PD-L1 pathway have shown clinical benefits [25,27]. Despite these advancements, significant challenges remain, especially in advanced stages [28–30]. Owing to the complex interactions between cytokines secreted by fibroblasts and stromal cells, the tumor microenvironment (TME) significantly contributes to NSCLC progression [31–34]. Growth factors such as hepatocyte growth factor (HGF), VEGF, epidermal growth factor (EGF), and osteopontin (OPN) promote epithelial-mesenchymal transition (EMT) via pathways such as the PI3K/AKT and mTOR, inducing stemness and facilitating drug resistance and metastasis [35]. However, the specific functions and molecular mechanisms of the cytokines produced by NSCLC cells, particularly stem-like tumor cells, are only beginning to be understood [36]. NSCLC progression and metastasis are associated with multiple signaling pathways, including the AKT/mTOR [37], Wnt/β-catenin [38], NF-κB/Snail [39], ERK1/2, and matrix metalloproteinase 9 (MMP9) [40]. Understanding how these cytokines modulate these pathways is crucial for unraveling the mechanisms underlying NSCLC progression and developing more effective treatments that simultaneously target these aberrantly activated pathways.

L-theanine, an amino acid found in tea plants, the mushroom *Xerocomus badius*, and some species of the genus Camellia, has been marketed as a dietary supplement in the United States and has shown potential benefits in alleviating the adverse effects of anticancer drugs and improving the quality of life for patients with colorectal cancer [41]. Our previous studies have indicated that L-theanine and its derivatives inhibit the migration and invasion of human lung cancer cells [42]. However, the parent compound L-theanine has a short half-life and limited efficacy, leading to challenges related to its druggability. In addition, given the ease of lung cancer cell metastasis, derivatives of L-theanine with both potent efficacy and whole-body distribution have not been obtained.

In this study, we developed and synthesized a new and more potent L-theanine derivative, ethyl 6-chlorocoumarin-3-carboxylyl L-theanine (TClC), derived from L-theanine and coumarin, and systematically evaluated its therapeutic efficacy against NSCLC both *in vitro* and *in vivo*, especially for metastasis. We demonstrated that TClC is more effective than L-theanine and its other derivatives that we previously reported against cancer invasion [43,44]. In particular, we utilized a comprehensive suite of target identification techniques to identify the molecular targets of TClC in highly invasive and metastatic NSCLC cells, revealing its strong anticancer effects as a polypharmacological agent over well-known small molecule inhibitors (AKT inhibitors, NF-κB inhibitors, and PD-L1 inhibitors) and clinical cancer drugs (cisplatin and gefitinib). Our findings suggest that TClC may serve as a promising therapeutic agent for managing metastatic NSCLC.

2. Results

2.1. Synthesis of a novel small fluorescent compound, ethyl 6-chlorocoumarin-3-carboxylyl L-theanine (TClC)

In our previous studies, we demonstrated the anticancer properties of L-theanine (T), including its ability to inhibit cancer cell migration and invasion [43,44]. However, to increase the antitumor activity of L-theanine, further optimization of its chemical structure is necessary, particularly to improve its ability to target specific cancer pathways. Coumarin, a natural compound found in higher plants such as Rutaceae and Umbelliferae, as well as essential oils such as cinnamon bark, Cassia leaf, and lavender oil, has demonstrated anticancer activity against various types of cancers [45]. To harness the benefits of coumarin, we synthesized a novel small fluorescent compound, ethyl 6-chlorocoumarin-3-carboxylyl L-theanine (TClC), by optimizing the structure of the natural molecule L-theanine. This synthesis involved the esterification of

L-theanine's carboxyl group with ethanol and the acylation of its amino group with 6-substituted coumarin-3-carboxylic acid (ClC), as shown in Fig. 1A. The chemical structure of TClC was verified using nuclear magnetic resonance (NMR) spectroscopy and high-resolution mass spectrometry (HRMS), and the resulting spectra are displayed in Fig. S1. Notably, TClC exhibited robust fluorescence both *in vitro* and *in vivo*, as evidenced by its visible fluorescence in mouse tissues, including the lungs, 3 h after intraperitoneal injection, as depicted in Fig. 1B. Moreover, we captured images of TClC distribution at multiple time points - 1, 3, 6, 12, and 24 h post-administration- as depicted in Figs. S2D–E. This expanded timeline offers a more detailed distribution profile of TClC in nude mice. These characteristics highlight TClC's potential for use in both imaging detection and therapeutic applications.

2.2. TClC has significant antitumor effects on NSCLC and sensitizes tumors to clinical chemotherapy agents

To assess the potential anticancer activity of TClC, we first employed an *ex vivo* method of serum pharmacology. This practical approach allows rapid assessment of the potential effects of a compound on animal or human tumor cell growth, migration, and invasion, which we reported previously [44,46,47]. In brief, rats were given vehicle control, L-theanine (T), ClC, or TClC, and then, the sera of drug-treated rats were obtained at various time points, as indicated in Fig. 1C, and mixed with

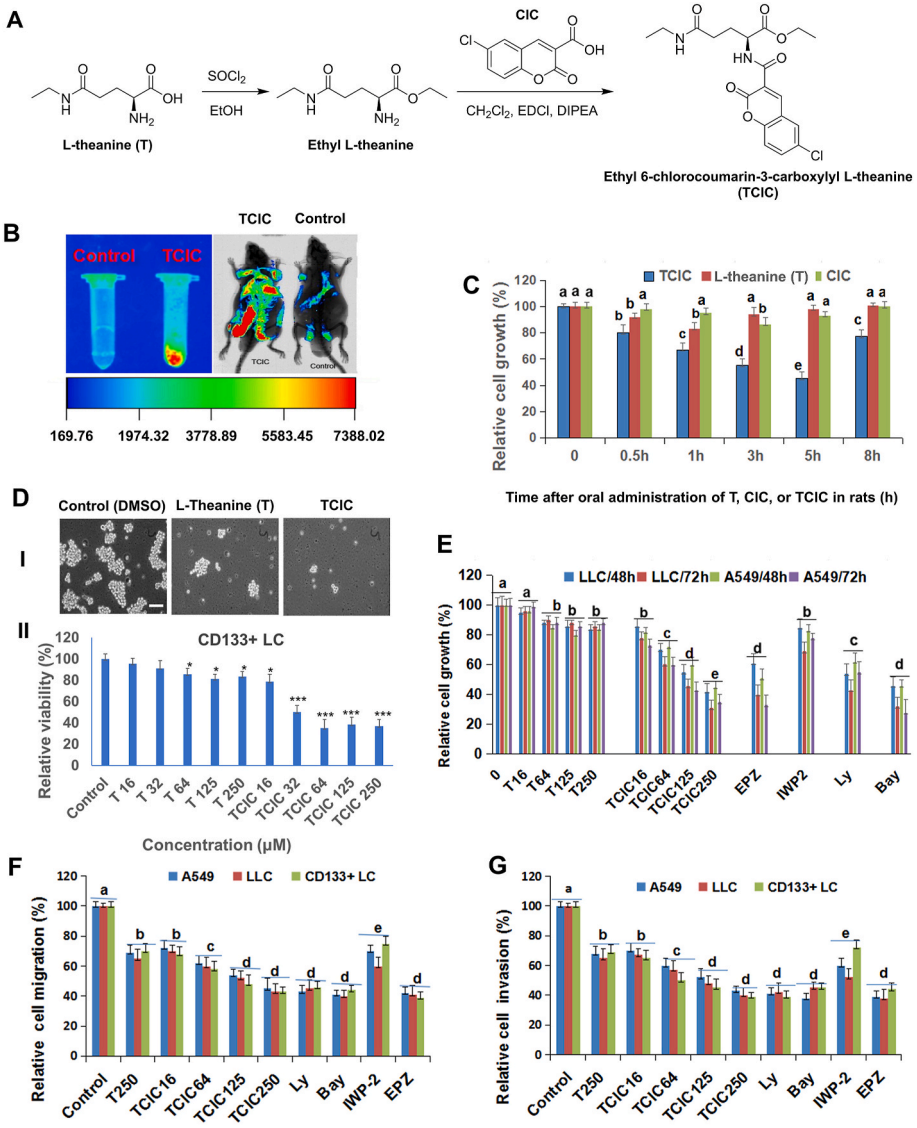

Fig. 1. Semisynthesis of ethyl 6-chlorocoumarin-3-carboxylyl L-theanine (TClC) and its inhibitory effects on the growth, migration, and invasion of NSCLC cells. (A) TClC was prepared as outlined in the scheme. L-theanine (T) was treated with $SOCl_2$ in ethanol to generate ethyl L-theanine, which subsequently reacted with ethyl 6-chlorocoumarin-3-carboxylic acid (ClC) to generate TClC. The final product TClC was purified by column chromatography, and the structure was characterized by ^{1}H NMR, ^{13}C NMR and HRMS (Figs. S1A–C). **(B)** Detection of fluorescent signals of TClC *in vitro* and *in vivo*. TClC produced in tubes (left; 8 mg/mL) and *in vivo* (right) fluorescent signals (3 h after injection of TClC in mice (80 mg/kg/i.p.). **(C)** *Ex vivo* effects of sera from TClC-, T- or ClC-treated rats at 0, 0.5, 1, 3, 5 and 8 h after oral administration of TClC, T, or ClC on A549 cell growth. **(D)** The reduction in CD133+ LC cell sphere formation and viability induced by T and TClC. The CD133+ LC 3D spheres were treated with vehicle control (DMSO), L-theanine (T, 16–250 μM) or TClC (16–250 μM) for 4 days. The trypan blue exclusion test (TBET) confirmed that CD133+ LC sphere formation **(I)** and viability **(II)** were significantly inhibited by treatment with L-theanine (T) and TClC (scale bar = 100 μm). **(E–G)** Inhibition of cell growth in NSCLC A549 and LLC cell lines **(E)** as well as migration **(F)** and invasion **(G)** in A549, LLC, and CD133+ LC cells by L-theanine (T) and TClC in a dose-dependent manner (16–250 μM) as well as by inhibitors of the PI3K/AKT (Ly), NF-κB (Bay), β-catenin (IWP-2), and EZH2 (EPZ) signaling pathways. Different letters (a, b, c, d, e) indicate statistically significant differences between treatments ($p < 0.05$). The data are presented as the mean ± SEM (n = 3).

cell culture medium at a concentration of 10 %. Then, NSCLC cells cultured with this medium were subjected to a cell growth detection assay. Our results revealed that TClC-treated rat sera strongly inhibited NSCLC A549 cell growth even 8 h after TClC administration, with the peak inhibitory rate exceeding 55 % at 5 h. In contrast, L-theanine (T)- or ClC-treated rat sera significantly inhibited tumor growth only 1 h after drug administration, with peak inhibitory rates of approximately 18 % for T and 13 % for ClC (Fig. 1C). These data suggest that TClC has stronger suppressive effects on lung cancer cell growth than L-theanine or ClC does. Thus, in the subsequent experiments of this study, L-theanine was used as a parental "control" to elucidate the role of its derivative TClC and its molecular mechanism of action against NSCLC.

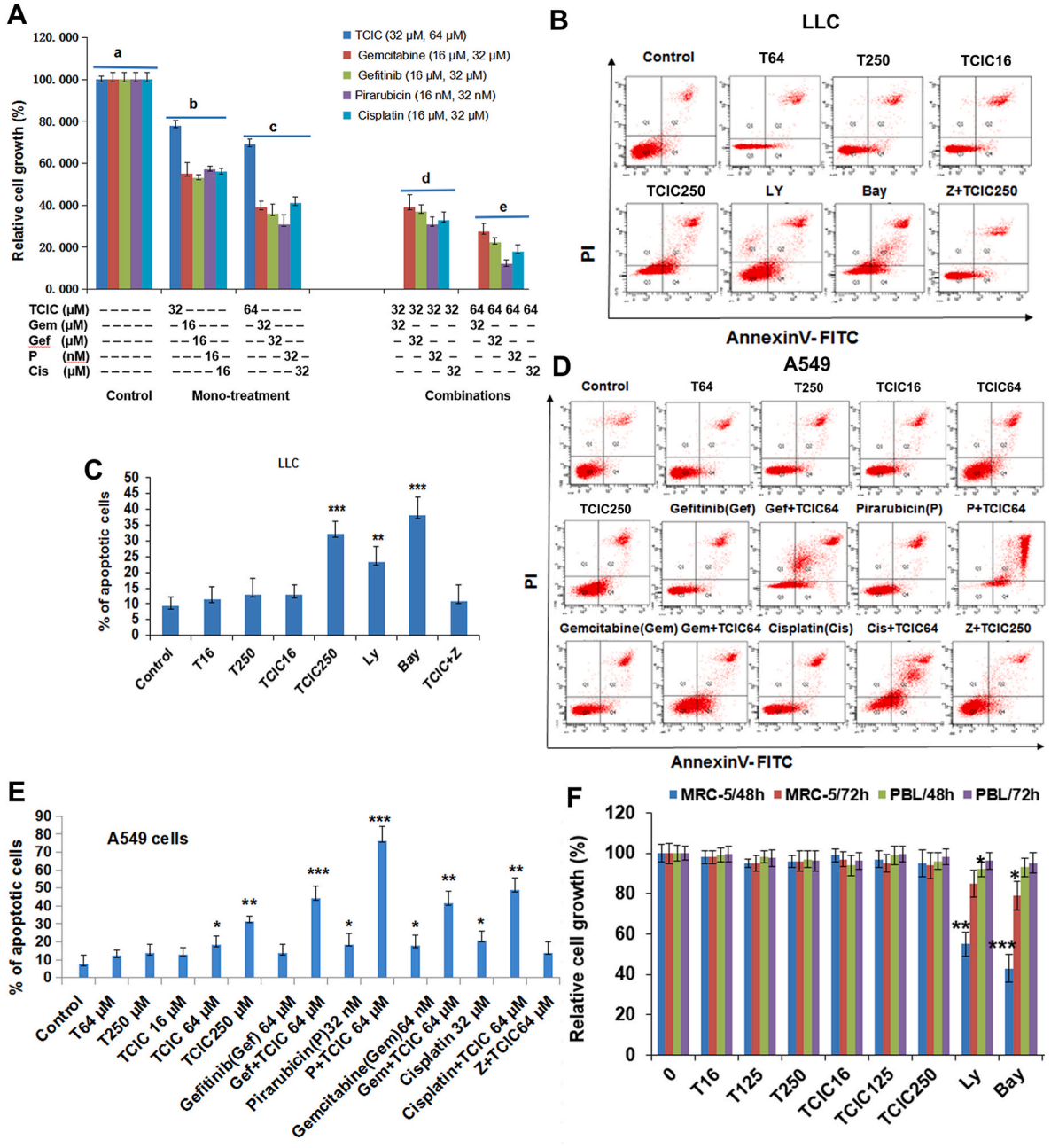

Fig. 2. TClC in combination with anticancer drugs enhances the growth inhibition of NSCLC cells and induces cell apoptosis without affecting normal cell growth. (A) A549 cells were incubated in complete medium supplemented with the indicated concentrations of TClC (32 or 64 μM) in combination with cancer drugs (gemcitabine at 16 or 32 μM, gefitinib at 16 or 32 μM, cisplatin at 16 or 32 μM, and pirarubicin at 16 or 32 nM). After drug treatment, the absorbance values in each test group were measured using the MTT assay. MTT assays confirmed the enhanced growth inhibition of A549 cells by TClC in combination with the first-line anticancer drugs gefitinib (32 μM), cisplatin (32 μM), pirarubicin (32 nM), or gemcitabine (32 μM). **(B–E)** Flow cytometry analysis of cell apoptosis in the NSCLC cell lines LLC **(B–C)** and A549 **(D–E)** after the cells were treated for 48 h with the indicated concentrations of TClC and L-theanine (T). The percentages of apoptotic LLC **(C)** and A549 **(E)** cells treated with TClC and L-theanine (T) are summarized. A PI3K/AKT inhibitor (Ly) and an NF-κB inhibitor (Bay), used as positive controls, also induced apoptosis in LLC and A549 cells. The caspase-3 inhibitor Z-VAD-FMK (Z) at 15 μM, the negative control, blocked apoptosis in TClC-treated LLC and A549 cells. **(F)** Treatment with TClC or L-theanine (T) (16–250 μM) had no significant effect on the growth of normal human peripheral blood lymphocytes (PBLs) or human embryonic lung fibroblast MRC-5 cells, but Ly (25 μM) and Bay (3.2 μM) significantly inhibited the growth of both cancer cells and normal PBLs and MRC-5 cells. The data are presented as the mean ± SEM (n = 3). Different letters (a, b, c, d, e) indicate statistically significant differences between treatments ($p < 0.05$). *, $p < 0.05$; **, $p < 0.01$; ***, $p < 0.001$, *vs* control.

To confirm the anticancer effects of TClC in NSCLC, we evaluated the TClC-mediated regulation of cell growth, migration, and invasion in CD133+ cells isolated from A549 cells (CD133+ LC cells), which are relatively insensitive to several cancer drugs, such as cisplatin and gefitinib [48,49]. Flow cytometry analysis revealed that CD133 expression was greater in CD133+ LC cells than in parental A549 cells (66.2 % *vs* 5.3 %, Fig. S2A I-II). A 3D sphere-forming assay revealed that 3D spheres formed from isolated CD133+ LC cells (Fig. S2A III) but not from A549 cells (Fig. S2A IV). Interestingly, compared with L-theanine, TClC markedly reduced CD133+ LC sphere formation (Fig. 1D I) and viability (Fig. 1D II), although its effect on CD133+ LC cell viability remained unchanged with increasing dose, which can be attributed to the saturation effect of the TClC dose.

We next measured the effects of TClC on tumor cell growth,

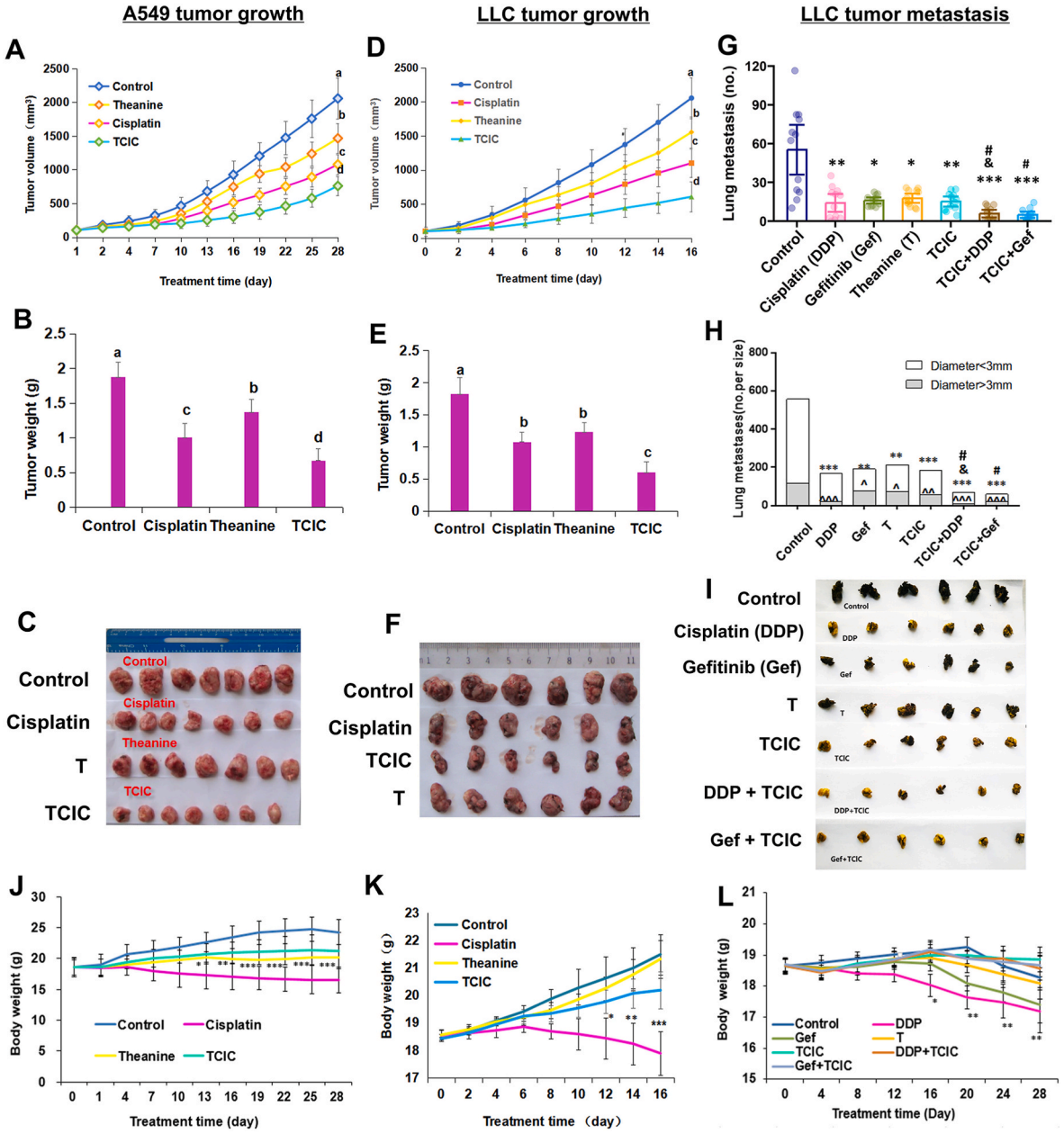

Fig. 3. *In vivo* inhibition of A549 and LLC xenograft tumor growth and lung metastasis by TClC as a single agent or combination therapy with clinical drugs. A549 and LLC cells were transplanted into the right flank of each mouse. After 10–15 days, the tumor growth models were established, and drug treatment began. For the LLC metastasis experiment, LLC cells were injected into the tail vein of each mouse, and drug treatment began the next day. The tumor-bearing mice were randomly divided into the different groups indicated in figure. **(A, D)** Changes in tumor volume. Changes in tumor volume were recorded for each treatment group over the course of the experiment. **(B, E)** Tumor weight. Tumor weights were measured at the end of the experiment for each treatment group. **(C, F)** Photographs of excised tumors from each treatment group were taken for comparison. **(G–I)** Suppression of LLC metastasis. LLC metastasis was suppressed by L-theanine (T) and TClC, and this suppression was enhanced when TClC was combined with cisplatin (DDP) or gefitinib (Gef) in the lungs of mice. Total number of metastatic nodules in the lungs of each mouse. **(G)** Size of metastatic nodules divided by size, including large (diameter ≥3 mm) and small (diameter <3 mm) nodules in the lungs of mice in each group **(H). (I)** Representative metastatic lung tissues from the mice. **(J, K, L)** Body weights of the mice during the course of treatment. Tumor volumes, weights and metastatic nodules were compared among groups using ANOVA and the Bonferroni post hoc test. The values are shown as the mean ± the standard error of the mean (SEM) for each group (n = 6–7). Values with different letters (a, b, c, d) indicate statistically significant differences between treatments ($p < 0.05$). * or ^, $p < 0.05$, ** or ^^, $p < 0.01$, *** or ^^^, $p < 0.001$, *vs.* Control; $^{\&}p < 0.05$, *vs.* DDP, Gef, T and TClC (for the large nodules); $^{\#}$, $p < 0.05$, *vs.* DDP, Gef, T and TClC (for the small nodules).

migration, and invasion using *in vitro* assays. TClC strongly reduced the relative growth rate (Fig. 1E), migration rate (Fig. 1F), and invasion rate (Fig. 1G) of NSCLC A549, LLC, and CD133+ LC cells. Similarly, inhibitors targeting PI3K/AKT (LY294002, Ly), NF-κB (BAY 11–7082, Bay), β-catenin (an inhibitor of Wnt production 2, IWP-2), and EZH2 (tazemetostat, EPZ), which were used as positive controls given the well-known oncogenic roles of these proteins, also significantly inhibited the growth, migration, and invasion of these NSCLC cells. We also tested the efficacy of TClC in the additional NSCLC line H460 and demonstrated its ability to suppress the growth of H460 cells (Fig. S2B).

Furthermore, TClC in combination with clinically used first-line cancer drugs, including gefitinib, cisplatin, gemcitabine, and pirarubicin, significantly enhanced the inhibition of A549 cell growth (Fig. 2A). Additionally, TClC induced apoptosis in LLC (Fig. 2B and C) and A549 (Fig. 2D and E) cells, surpassing the inhibitory effect of its parental compound, L-theanine. When TClC was combined with cancer drugs, it strongly enhanced the induction of cell apoptosis in A549 cells and significantly sensitized them to gefitinib, cisplatin, gemcitabine, and pirarubicin (Fig. 2D and E). The caspase 3 inhibitor Z-VAD-FMK, the negative control, eliminated TClC-induced apoptosis, demonstrating that TClC can induce apoptosis in both A549 and LLC cells (Fig. 2B–E). Importantly, TClC did not inhibit the growth of normal human peripheral blood lymphocytes (PBLs) or MRC-5 human embryonic lung fibroblasts at comparable concentrations (16–250 μM), while positive control inhibitors targeting PI3K/AKT (Ly, 25 μM) and NF-κB (Bay, 3.2 μM) significantly inhibited the growth of both cancer cells and normal PBLs and MRC-5 cells (Fig. 2F). Collectively, these data suggest that TClC strongly inhibits the growth, migration and invasion of NSCLC cells and the sphere-forming ability and viability of CD133+ LC cells.

2.3. TClC inhibits tumor growth and metastasis in NSCLC both as a single agent and in combination with chemotherapeutic drugs

We then evaluated the anticancer effects of TClC *in vivo* using both subcutaneous xenograft models and a metastasis model. Our findings revealed that TClC significantly reduced tumor growth in two different settings: in nude mice implanted with A549 xenografts and in immunocompetent mice implanted with LLC xenografts. Specifically, in the group of A549 tumor-bearing mice treated with TClC, we observed a marked decrease in both tumor volume and tumor weight, with reductions of 71.2 % and 64.3 %, respectively (Fig. 3A–C). Similarly, in LLC tumor-bearing mice treated with TClC, the relative inhibitory effects on tumor volume and tumor weight were 71.8 % and 67.1 %, respectively (Fig. 3D–F). Notably, TClC exhibited more than 2-fold greater efficacy in inhibiting A549 (Fig. 3A and B) and LLC (Fig. 3D and E) tumor growth than L-theanine alone. Furthermore, in a metastasis model in which LLC cells were injected through the tail vein, TClC (80 mg/kg/d) effectively suppressed lung metastasis. L-theanine (80 mg/kg/d), cisplatin (1.5 mg/kg/d), and gefitinib (250 mg/kg/d) had comparable suppressive effects on lung metastasis. Notably, TClC more strongly inhibited LLC metastasis than L-theanine or gefitinib did, even though the dose of gefitinib was 3-fold greater than that used for TClC (Fig. 3G–I). Additionally, when TClC was administered at a reduced dose of 40 mg/kg/d, the inhibition of metastasis significantly enhanced when TClC was combined with reduced doses of cisplatin (1.5 mg/kg/2 d) and gefitinib (250 mg/kg/2 d) compared with cisplatin or gefitinib alone at regular doses (Fig. 3G). The efficacy of TClC in inhibiting LLC metastasis in the lung was remarkable, as demonstrated by the relative inhibitory effects on large colonies (diameter $\geq$3 mm) and small colonies (diameter $<$3 mm) in the following groups: cisplatin treatment alone, 82.3 % and 66.6 %; gefitinib treatment alone, 34.9 % and 73.8 %; L-theanine treatment alone, 30.4 % and 69.5 %; TClC treatment alone, 51.6 % and 72.6 %; TClC in combination with cisplatin, 92.9 % and 86.2 %; and TClC in combination with gefitinib, 83.1 % and 91.2 %, respectively (Fig. 3H). Representative metastasized tumors from LLC tumor-bearing mice are shown in Fig. 3I. Moreover, TClC exhibited no toxicity in mice, as there was no significant change in body weight (Fig. 3J-L), while cisplatin and gefitinib led to a reduction in body weight. Taken together, these data suggest that TClC suppresses tumor growth and metastasis in mice more strongly than does its parental compound L-theanine. Additionally, TClC suppressed tumor metastasis in mice at a dose lower than that of the EGFR inhibitor gefitinib. Furthermore, unlike the administration of gefitinib or the alkylating agent cisplatin, TClC administration did not cause significant body weight changes in the mice. Importantly, TCIC accumulation is primarily observed in the tumor tissue (Figs. S2E–F), with minimal accumulation in other vital organs such as the liver, spleen, heart, lungs, and kidneys. This observation has been displayed by the dissection results at 24 h after treatment, as depicted in Figs. S2E–F. Finally, we have demonstrated that compared with the positive control dofetilide, TCIC has low effects on the hERG ion channel, which is critical for cardiac safety (Fig. S7).

2.4. TClC regulates key effectors in multiple signaling pathways in CD133+ NSCLC cells, driving a positive feedback autocrine loop involved in promoting NSCLC growth, progression, and metastasis

Cancer cells with stem-like properties that express high levels of stem cell surface markers, such as CD133, play crucial roles in regulating various cancer hallmarks through interactions with cells and the extracellular matrix (ECM) in the TME. These cells achieve this goal by secreting soluble factors, such as growth factors, into the TME and stimulating oncogenic and angiogenic signaling pathways as well as stemness-related pathways, creating an immunosuppressive environment [10,19,50,51]. To investigate the effects of culture supernatants from CD133+ LC cells, containing tumor-secreted factors, we compared CD133+ LC cells with A549 cells after 48 and 96 h of culture, with a specific focus on cell growth, migration, and invasion. After the cells were treated with medium containing 10 % FBS plus an equal volume of the supernatant (referred to as CSCM) of 48- (48 h-CSCM) or 96-h-cultured (96 h-CSCM) CD133+ LC cells for 24 h, the relative growth rates of the CD133+ LC and A549 cells were 116 % and 133 % (for CD133+ LC) and 145 % and 162 % (for A549 cells), compared with those of both control groups treated with 10 % FBS only (Fig. 4A). Compared with 48 h of culture, 96 h of culture increased the growth of both CD133+ LC and A549 cells, respectively. Additionally, in terms of migration and invasion rates, CD133+ LC cells demonstrated significantly greater migration and invasion than did A549 cells. When subjected to medium containing 10 % FBS plus an equal volume of the 48 h-CSCM, CD133+ LC cells had significantly greater relative rates of migration and invasion, with increases of 151 % and 171 %, respectively, compared with those of A549 cells (110 % and 118 %). Notably, the addition of the supernatant from 96-h-cultured CD133+ LC cells (96 h-CSCM) to 10 % FBS medium resulted in even greater relative rates of migration and invasion. Specifically, compared with A549 cells treated with only 10 % FBS, CD133+ LC cells exhibited marked increases (162 % and 188 %) in migration and invasion, respectively, while A549 cells showed increases (125 % and 138 %) in migration and invasion, respectively (Fig. 4B and C, Table 1).

Given the critical roles of HGF, EGF, VEGF, OPN, and MMP9 in the NSCLC microenvironment for cancer invasion and progression [34], we performed ELISA analysis of the secreted proteins to assess the differences in culture supernatants between CD133+ LC and A549 cells. As shown in Table 1, the secreted protein levels of HGF, EGF, VEGF, OPN, and MMP9 increased by approximately 1.3- to 1.4-fold in the supernatants of both cell types over the culture period. Importantly, the supernatants of CD133+ LC cells presented significantly greater levels of these proteins than did those of A549 cells. The secreted protein levels in CD133+ LC cells increased significantly, with a 27-fold increase in HGF, a 102-fold increase in EGF, a 2.8-fold increase in VEGF, a 1.2-fold increase in OPN, and a 4.6-fold increase in MMP9 compared with those in A549 cells cultured for 48 h. Furthermore, these protein levels were greater in both CD133+ LC cells and A549 cells cultured for 96 h than in

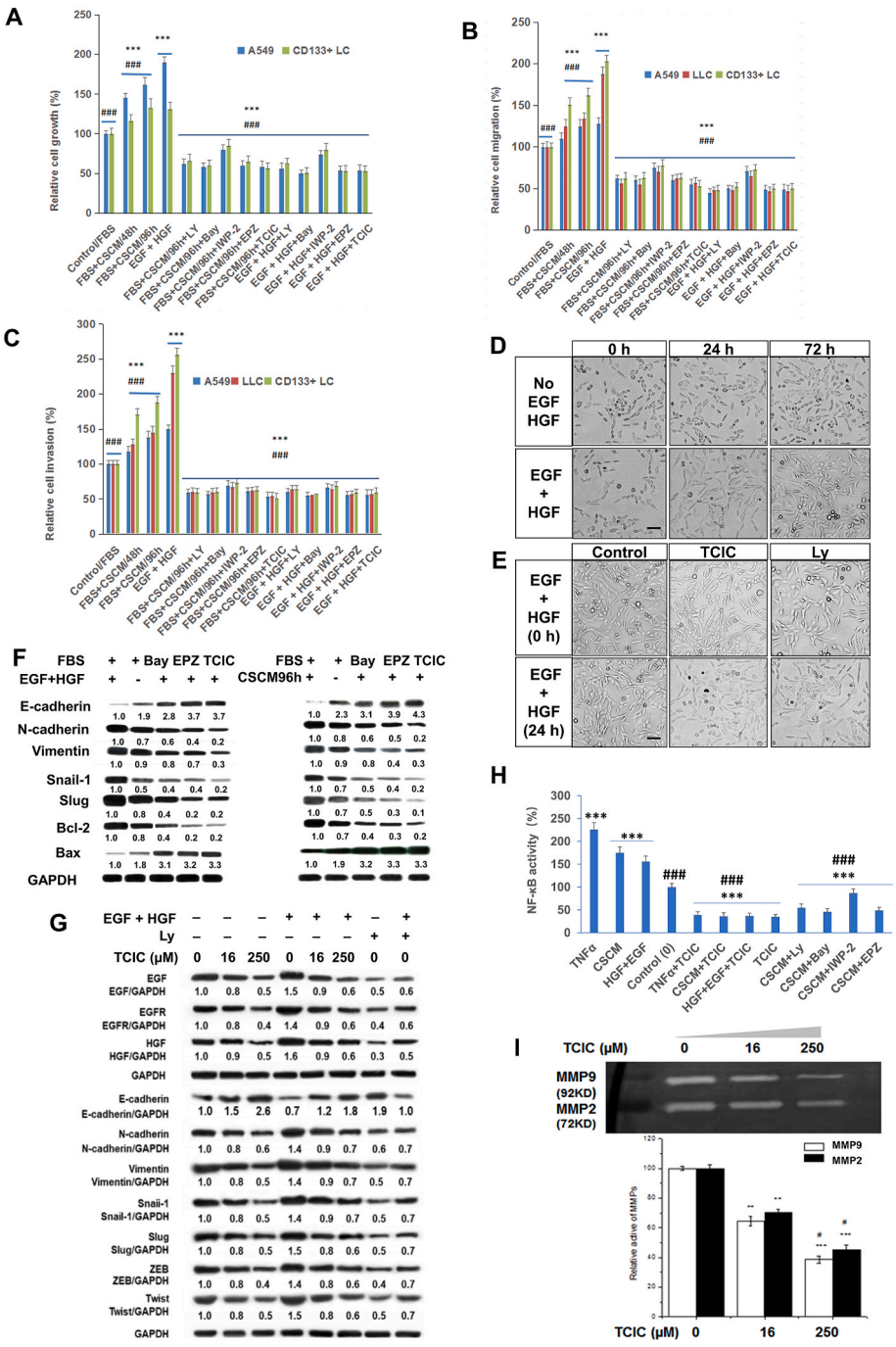

Fig. 4. Effects of TClC and related inhibitors on FBS + CSCM- and EGF + HGF-enhanced NSCLC cell growth, migration, invasion, EMT and relevant protein expression. (A–C) Inhibition of cell growth, migration, and invasion. In the presence of 10 % FBS, and the supernatants of 48-h-(48 h-CSCM) or 96-h-(96 h-CSCM)-cultured CD133+ LC cells and/or EGF + HGF, the increase in relative cell growth **(A)**, migration **(B)** and invasion **(C)** of CD133+ LC and NSCLC A549 and LLC cells was significantly suppressed by the inhibitors, Ly (LY294002, a PI3K/AKT inhibitor), Bay (Bay11-7082, an NF-κB inhibitor), IWP-2 (a β-catenin inhibitor), EPZ (tazemetostat, an EZH2 inhibitor) and TClC. **(D–G)** Effects on EMT, apoptosis, and morphological changes. EGF + HGF- and/or FBS + CSCM (96 h)-enhanced alterations related to EMT and apoptosis in CD133+ LC or A549 cells and morphological changes. **(D)** A549 cells treated with EGF and HGF are shown at 0, 24, and 72 h. **(E)** TClC treatment inhibited EGF + HGF-induced mesenchymal transition in A549 cells. Ly was used as a control. EGF + HGF- and/or FBS + CSCM (96 h)-enhanced alterations related to EMT and apoptosis in CD133+ LC (**F**) or A549 (**G**) cells were completely reversed by Bay, IWP-2, EPZ, Ly and/or TClC (scale bar = 200 μm). (**H**) Suppression of NF-κB activation. TNF-α-induced, CSCM (96 h)- and/or EGF + HGF-enhanced nuclear transcriptional activation of NF-κB p65 in CD133+ LC cells was significantly suppressed by Ly, Bay, IWP-2, EPZ and TClC. **(I)** Inhibition of MMP activity. MMP9 and MMP2 activities in A549 cells were inhibited by TClC. The figures represent three similar experimental results. The data are presented as the mean ± SEM (n = 3 biological replicates). **, $p < 0.01$; ***, $p < 0.001$, *vs.* control; $^{###}$, $p < 0.001$, *vs.* EGF + HGF/CSCM/TNF-α.

Table 1
The protein levels of EGF, HGF, VEGF, OPN and MMP9 in the supernatant, and the rates of the migration, invasion and growth of A549 cells and CD133+ lung cancer cells (CD133+ LC).

Cells	Factors							
	HGF (pg/mL)	EGF (pg/mL)	OPN (pg/mL)	VEGF (pg/mL)	MMP9 (pg/mL)	Relative migration (%)	Relative invasion (%)	Relative growth (%)
A549 (48 h)	58 ± 5	12 ± 3	552 ± 38	318 ± 21	32 ± 3	100 ± 6[a]	100 ± 5[a]	100 ± 4[a]
CD133+ LC (48 h)	1610 ± 86 ***	1226 ± 59 ***	660 ± 52 **	902 ± 46 ***	(150 ± 12) × 10^3 ***	151 ± 11[a] ***	171 ± 10[a] ***	80 ± 9[a] *
A549 (96 h)	75 ± 6 *	15 ± 4 *	635 ± 41 *	379 ± 24 *	40 ± 4 *	125 ± 8[b] ***	138 ± 9[b] **	112 ± 16[b] ***
CD133+ LC (96 h)	2238 ± 98 ***##	1607 ± 93 ***#	875 ± 72 **###	1180 ± 82 ***##	(198 ± 17) × 10^3 ***###	162 ± 9[b] ***###	188 ± 8[b] ***###	91 ± 11[b] ***##

*, $p < 0.05$; **, $p < 0.01$; ***, $p < 0.001$, *vs* A549 (48 h); #, $p < 0.05$; ##, $p < 0.01$; ###, $p < 0.001$, *vs* CD133+ LCSCs (48 h).
[a] Results of cell treatment for 6 h (migration)/20 h (invasion) with 10 % FBS in medium as a chemoattractant in the lower chamber or cell treatment for 24 h (growth) with 10 % FBS in medium plus an equal volume of the supernatant of 48 h CD133+ LC.
[b] Results of cell treatment for 6 h (migration)/20 h (invasion) with 10 % FBS containing medium plus an equal volume of the supernatant of CD133+ LCs cultured for 96 h as a chemoattractant in the lower chamber or cell treatment for 24 h (growth) with 10 % FBS-containing medium with an equal volume of the supernatant of 96 h CD133+ LCs. The values are shown as the mean ± SEM for each group; n = 3 biological replicates.

those cultured for 48 h. These findings indicate that CD133+ LC cells exhibit stronger migratory and invasive capabilities than A549 cells, possibly resulting from the enhanced levels of secreted proteins, including HGF, EGF, VEGF, OPN, and MMP9.

Building upon the identification of EGF and HGF as potential tumor inducers from CD133+ LC supernatants (CSCMs) as well as the relevant signaling pathways, we further determined whether TClC and the inhibitors associated with signaling pathways could inhibit the tumor progression potential induced by EGF and HGF. To evaluate this possibility, we compared the differential effects of TClC with those of related inhibitors and of EGF plus HGF. MTT assays revealed that TClC significantly inhibited the growth of both CD133+ LC and A549 cells, compared with that of control cells treated with medium containing only 10 % FBS. After treating the cells with medium containing 10 % FBS supplemented with EGF plus HGF, the relative growth rates of the CD133+ LC and A549 cells increased by 131 % and 190 %, respectively. TClC reduced the relative growth rate induced by EGF plus HGF by 53 % (CD133+ LC) and 54 % (A549) (Fig. 4A). Similarly, upon treating the cells with medium containing 10 % FBS supplemented with EGF plus HGF, the relative migration rates of the CD133+ LC and A549 cells increased by 203 % and 128 %, respectively, and the migration of the CD133+ LC cells increased more than that of the A549 cells. TClC reduced the relative rate of cell migration induced by EGF plus HGF by 49 % (CD133+ LC) and 50 % (A549) (Fig. 4B). Additionally, upon treating the cells with medium containing 10 % FBS supplemented with EGF plus HGF, the relative invasion rates of the CD133+ LC and A549 cells increased by 256 % and 150 %, respectively, and CD133+ LC promoted greater invasion than did the A549 cells. TClC reduced the relative rate of cell invasion induced by EGF plus HGF by 59 % (CD133+ LC) and 56 % (A549) (Fig. 4C). More importantly, the TClC-mediated anticancer effects were comparable to those of single specific inhibitors of PI3K/Akt (Ly), NF-κB (Bay), β-catenin (IWP-2), and EZH2 (EPZ) (Fig. 4A–C), suggesting that TClC functions as a multiple-target inhibitor in NSCLC cells.

EMT is implicated in the conversion of early-stage tumors into invasive malignancies. The acquisition of migratory and invasive abilities by cells has long been considered a hallmark of EMT and is often used as a surrogate to describe the role of EMT in metastasis [52]. Therefore, we investigated whether TClC could prevent EGF plus HGF-induced EMT. Treatment with TClC reversed EGF + HGF-induced EMT, as indicated by morphological changes and alterations in the expression of related proteins in A549 cells (Fig. 4D–G). The microscopy results revealed that NSCLC cells gradually displayed a fibroblastic morphology after treatment with EGF and HGF for 24 or 72 h (Fig. 4D), and TClC treatment inhibited the mesenchymal phenotype induced by 24 h of treatment with EGF + HGF (Fig. 4E). As shown by Western blotting, EGF + HGF downregulated E-cadherin protein expression while upregulating the protein expression of EGF, HGF, EGFR, and EMT marker proteins and the related transcription factors N-cadherin, vimentin, snail-1, slug, ZEB, and Twist in A549 cells. Similarly, FBS + CSCMs strongly downregulated the protein expression of E-cadherin and Bax while upregulating the protein expression of N-cadherin, vimentin, snail-1, and Bcl-2 in CD133+ LC cells (Fig. 4F). TClC, Bay, EPZ, and/or Ly inhibited the expression of these EMT markers induced by EGF + HGF and/or FBS + CSCM, leading to increased E-cadherin and Bax expression, regardless of the presence or absence of exogenous EGF + HGF and/or FBS + CSCM (Fig. 4F and G).

Additionally, NF-κB activation promotes tumor cell proliferation, survival, inflammation and immune escape, and induces or mediates the expression of many tumor-associated genes [53–56]. We then evaluated the inhibitory effect of TClC on NF-kB activity via the nuclear transcriptional activation of NF-κB induced by TNF-α [57], FBS + CSCM, and EGF + HGF in CD133+ LC (Fig. 4H) and A549 (Fig. S2C) cells. Similarly, the inhibitors Ly, Bay, IWP-2, and EPZ also inhibited FBS + CSCM-enhanced NF-κB activity in CD133+ LC and A549 cells (Fig. 4H and Fig. S2C). Furthermore, matrix metalloproteinases (MMPs) are key factors involved in tumor progression, metastasis and stemness [58]. We found that TClC suppressed MMP9 and MMP2 activity in A549 cells (Fig. 4I), suggesting its potential to prevent tumor progression and metastasis.

Collectively, the data described above demonstrate that CD133+ LC cells secrete elevated levels of oncogenic factors, including HGF and EGF, as well as VEGF, OPN, and MMP9, in the CSCM, contributing to a pro-tumorigenic/metastatic positive autocrine feedback loop in NSCLC through multiple related signaling pathways. These findings provide compelling evidence that TClC inhibits FBS + CSCM- and EGF + HGF-enhanced EMT, growth, migration, and invasion, as well as the modulation of signaling pathways involving PI3K/Akt, NF-κB, β-catenin, and EZH2 in NSCLC.

2.5. EZH2, β-catenin, AKTs, NF-κB, and PD-L1 are binding targets of TClC, highlighting TClC as a polypharmacological inhibitor

To elucidate the involvement of the aforementioned multiple signaling pathways in the anticancer activity of TClC, we conducted a comprehensive molecular structural investigation to identify the binding targets of TClC. Utilizing molecular dynamics (MD) simulations, we found that TClC consistently anchored the binding pockets of EZH2, NF-κB, AKT1, AKT2, β-catenin, and PD-L1 (Fig. 5A and Supporting Information). TClC, synthesized from coumarin and L-theanine, preferentially forms hydrogen bonds with polar residues via the lactone ring in the coumarin moiety. Additionally, the benzene and theanine moieties

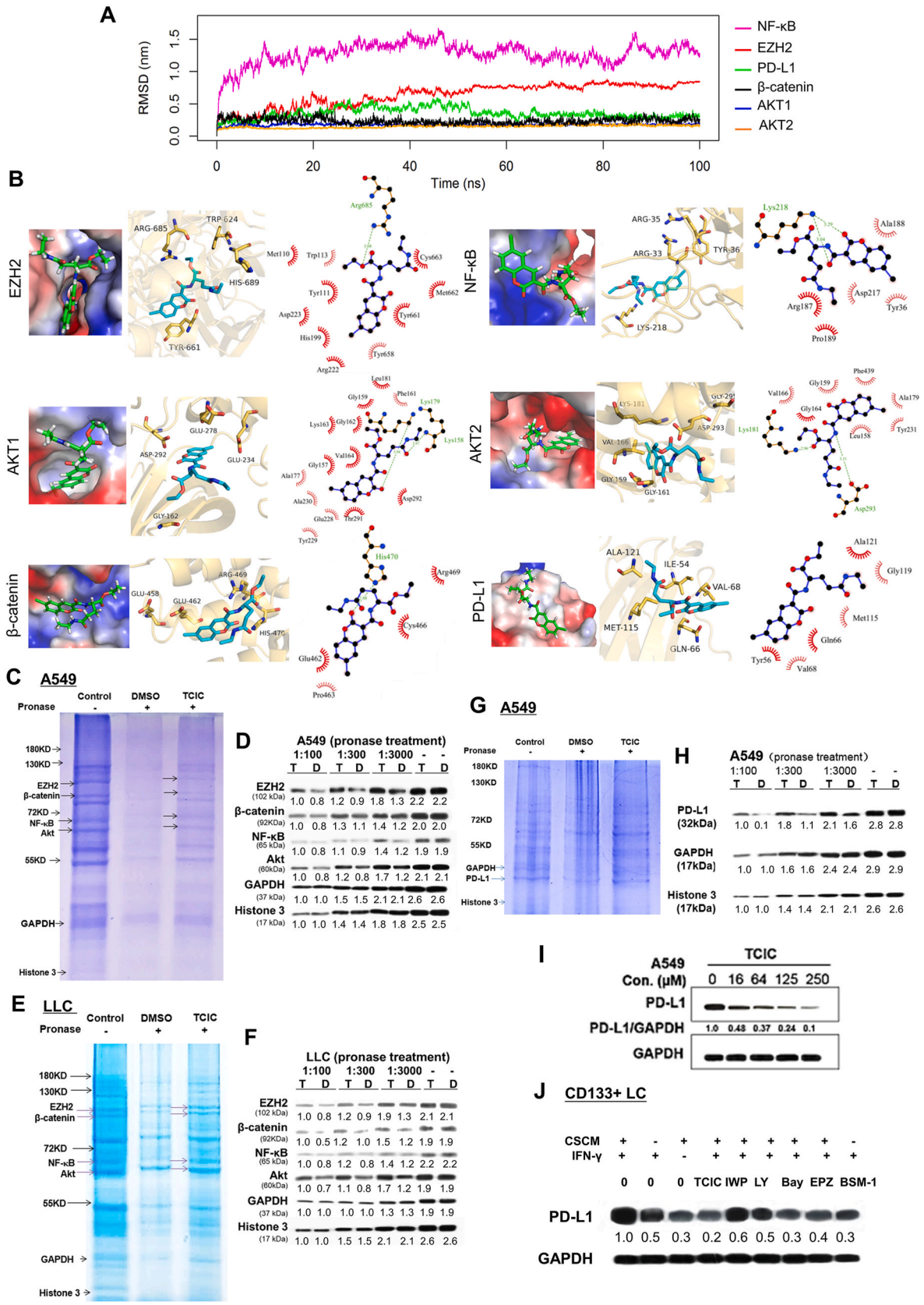

(caption on next page)

Fig. 5. Identification of EZH2, NF-κB, AKTs, β-catenin and PD-L1 as functional binding targets of TClC. (A) MD simulations of TClC and six targets. The RMSD values of EZH2 (red), NF-κB (magenta), AKT1 (blue), AKT2 (orange), PD-L1 (green) and β-catenin (black) were calculated from the backbone after least squares fitting to the backbone. **(B)** Representative conformations and binding modes of TClC to its target proteins EZH2, NF-κB, AKT1, AKT2, PD-L1, and β-catenin. The green sticks represent conformations of TClC. The protein surfaces are colored according to their electrostatic potentials, from red (−63.786) to blue (63.786) for EZH2, from red (−63.410) to blue (63.410) for NF-κB, from red (−63.398) to blue (63.398) for AKT1, from red (−70.081) to blue (70.081) for AKT2, from red (−61.260) to blue (61.260) for PD-L1, and from red (−59.190) to blue (59.190) for β-catenin. The binding modes of TClC to its targets were as follows: target (golden sticks and cartoon) and TClC (cyan stick). Amino acid residues in the target proteins that interact with TClC via hydrogen bonds are shown with text and dotted lines in green. Amino acid residues that are involved in hydrophobic contacts with TClC were shown with black text and red arches with bristles. **(C–H)** Binding validation by DARTS and Western Blotting. EZH2, β-catenin, NF-κB, AKT and PD-L1 were identified as TClC binding proteins in A549 **(C-D, G-H)** and LLC **(E–F)** cells, as determined by DARTS (**C, E, G**) and Western blotting (**D, F, H**) results. As shown in **C, E and G**, compared to those in the control group not treated with pronase, where EZH2, β-catenin, NF-κB, Akt, and PD-L1 exhibited the highest density, the TClC group and DMSO group treated with pronase exhibited high and low density, respectively. As shown in **D, H and F**, different concentrations of pronase (dilutions of 1:100, 1:300, 1:3000 and without pronase treatment) were used, showing that TClC (T group) and DMSO (D group) affected the protein densities of EZH2, β-catenin, NF-κB, AKT, and PD-L1, but not the housekeeping proteins GAPDH and histone-3. **(I)** TClC decreased PD-L1 expression in A549 cells in a dose-dependent manner. GAPDH served as a loading control. The intensity of PD-L1 expression was quantified using ImageJ and is shown as values ranging from 0 to 1 under the PD-L1 bands. **(J)** Effects of TClC and the inhibitors IWP-2, Ly, Bay, EPZ, and BMS-1 on the INF-γ-induced and CSCM-enhanced protein expression of PD-L1 in CD133+ LC cells. INF-γ-induced and/or CSCM (96 h)-enhanced PD-L1 expression in CD133+ LC cells was completely reversed by Ly, Bay, IWP-2, EPZ and TClC. The figures represent three similar experimental results.

readily engaged in hydrophobic interactions with key residues within the targets (Fig. 5B). Notably, the representative conformations of TClC (Fig. 5B) exhibited similar binding modes and affinities comparable to those of the positive controls EPZ (an EZH2 inhibitor), BMS-1 (a PD-L1 inhibitor), Bay (an NF-κB inhibitor), Ly (a PI3K/Akt inhibitor), and IWP-2 (a β-catenin inhibitor) (Figs. S4A–F and Table S1).

In the case of EZH2 binding, the coumarin group of TClC inserted into the cavity formed by Tyr111 and Tyr661 [59], while the oxygen atom in TClC established a hydrogen bond with Arg685 (Fig. 5B). In the case of NF-κB binding, the oxygen atoms in TClC formed a bifurcated hydrogen bond with Lys218 (Fig. 5B), one of the key acetylation and methylation sites of NF-κB involved in its binding to IκBα and other enhancers [60]. The branched groups of TClC interacted with the phosphate-binding loop (P-loop) region, engaging in a hydrogen bond with Lys158 in AKT1 and were situated adjacent to the DFG (Asp293-Phe294-Gly295) motif by forming hydrogen bonds with Lys181 and Asp293 in AKT2 (Fig. 5B). TClC also established multiple hydrophobic interactions within the binding pocket of PD-L1 and β-catenin (Fig. 5B). In contrast, although coumarin and L-theanine could access the binding pockets of these targets, their binding affinity was significantly lower than that of TClC, primarily due to their smaller volume and fewer interactions with key residues within the targets (Fig. 5B and S3, Table S2). This provides the theoretical basis for the superior antitumor activity of TClC compared with coumarin and L-theanine.

To validate the binding of TClC to the aforementioned targets in NSCLC, we conducted modified drug affinity responsive stability (DARTS) experiments, as previously described by us and others [61–63]. DARTS is a method that capitalizes on the fact that drug-protein binding complexes induce conformational changes in proteins, resulting in reduced sensitivity to proteases and protection from proteolysis, akin to the classical RNA protection assay. This approach effectively identifies target proteins that directly bind to a compound by subjecting cell lysates containing thousands of proteins to random mixing with the compound of interest, such as TClC. Using the DARTS method, we previously successfully identified nucleolin as a binding protein for the anticancer stem cell compound salinomycin in neuroblastoma cells [61]. In this study, both LLC and A549 cells were treated with vehicle (0.05 % DMSO) or TClC in the absence (control group) or presence of various concentrations of pronase (1:100, 1:300, 1:3000), followed by protein detection (Fig. 5C–H). The bands representing TClC-binding proteins in A549 cells (Fig. 5C and G) and LLC cells (Fig. 5E) were more intense after treatment with TClC + pronase than after treatment with DMSO + pronase. These findings indicate that TClC effectively protects its binding target proteins from pronase-mediated degradation in TClC-treated samples. Furthermore, Western blotting analysis using specific antibodies against EZH2, AKT, NF-κB, β-catenin and PD-L1 revealed increased protein levels in A549 cells and LLC cells after treatment with TClC + pronase at different pronase concentrations (1:100, 1:300, and 1:3000) compared with those in cells treated with DMSO + pronase at the same pronase concentrations (Fig. 5D, F, and H). Notably, TClC did not bind to the controls, histone 3 or the housekeeping protein GAPDH (Fig. 5D, F, and H). Together, these results unequivocally confirmed the identification of EZH2, AKT, NF-κB, β-catenin and PD-L1 as binding partners for TClC in A549 and LLC cells.

To confirm the abovementioned findings, we further conducted biochemical assays, including surface plasmon resonance (SPR) spectroscopy and thermal shift assay (TSA), to demonstrate the binding of TClC to two key players in NSCLC, EZH2 and PD-L1 (Figs. S5A–B), validating the authenticity of these target proteins of TClC. Moreover, considering the emerging importance of the PD-1/PD-L1 signaling pathway in lung cancer, the impact of TClC on PD-L1 expression was investigated. The experimental findings demonstrated that TClC effectively suppressed PD-L1 expression in highly metastatic melanoma B16F10 cells (Fig. S5C) and A549 cells (Fig. 5I) in a dose-dependent manner. Importantly, given that interferon-γ (INF-γ)-driven NF-κB stimulates PD-L1 expression [64], we further tested the inhibitory effects of TClC on CSCM-enhanced and INF-γ-induced PD-L1 expression in CD133+ LC cells and found that the suppression of PD-L1 expression induced by TClC was greater than that induced by the inhibitors of AKT (Ly), β-catenin (IWP-2), and PD-L1 (BMS-1) (Fig. 5J). Collectively, these results provide robust evidence that TClC, a polypharmacological inhibitor, binds to AKT1/2, EZH2, NF-κB, β-catenin and PD-L1 in NSCLC cells and can effectively suppress PD-L1 expression in CD133+ LC cells via CSCM activation and INF-γ induction.

2.6. TClC downregulates the expression of key oncogenic proteins and cancer stem cell markers simultaneously in NSCLC

Next, we investigated the molecular mechanisms underlying the anticancer effects of TClC in NSCLC by conducting loss-of-function assays on the oncogenic proteins AKT, NF-κB, EZH2, and β-catenin. The activation of these proteins has been implicated in the proliferation, migration, invasion, and metastasis in NSCLC [32,33,35,37–39]. Therefore, we examined the effects of knocking down AKT, NF-κB, β-catenin, and EZH2 via RNA interference (RNAi) or pharmacological suppression by protein inhibitors on the cellular functions of NSCLC and the expression of the tumor-secreted factors EGF, HGF, VEGF, and OPN, as well as cancer stem cell markers and the drug resistance-related proteins CD133, CD44, ALDH1, and ABCG2 [10,19,35,51].

As shown in Fig. 6, knockdown of AKT, NF-κB, β-catenin, or EZH2 also resulted in a 30 %–50 % reduction in the migration and invasion of both A549 and LLC cells. TClC suppressed A549 and LLC cell migration and invasion by approximately 50 % (Fig. 6A and B). Furthermore, TClC enhanced the inhibitory effects of single knockdowns on migration and invasion, whereas single knockdowns did not further enhance the

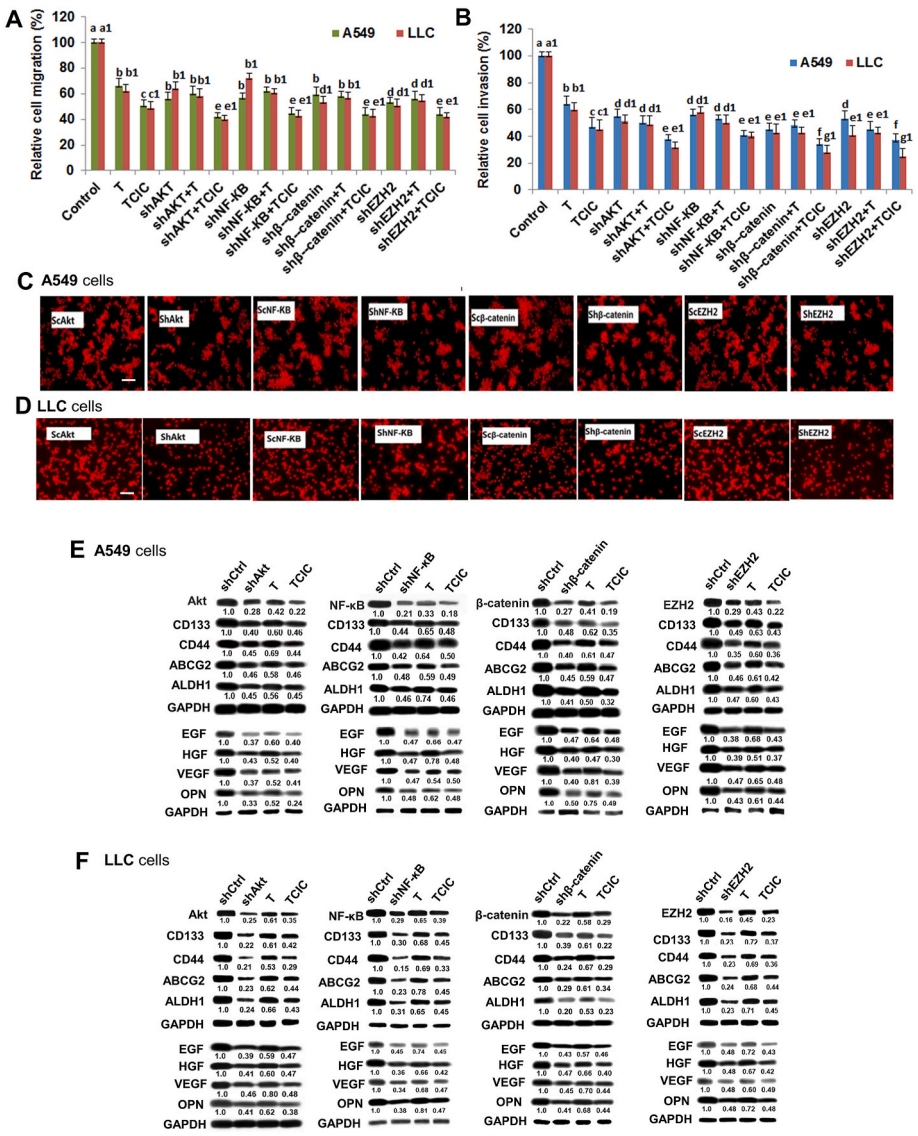

Fig. 6. Effects of knocking down AKT, NF-κB, β-catenin and EZH2 on cell growth, migration, invasion and the protein expression of EGF, HGF, VEGF, OPN, cancer stem cell markers and drug resistance proteins in NSCLC A549 and LLC cells. (A–C) The effects of knockdown of the AKT, NF-κB, β-catenin and EZH2 genes in combination with TClC and L-theanine (T) on migration **(A)** for 6 h and invasion **(B)** for 20 h in A549 cells. The figures represent three similar experimental results. The values are shown as the mean ± SEM for each group; n = 3 biological replicates. Values with different letters (a-g, a1-g1) indicate statistically significant differences between treatments ($p < 0.05$). **(C)** Images (scale bar = 50 μm) showing the reduced invasion of A549 cells stained with propidium iodide after the AKT, NF-κB, β-catenin and EZH2 genes were knocked down. **(D)** Images (scale bar = 50 μm) showing the reduced invasion of LLC cells stained with propidium iodide after the Akt, NF-κB, β-catenin and EZH2 genes were knocked down. Different letters (a-g, a1-g1) indicate statistically significant differences between treatments ($p < 0.05$). **(E–F)** Western blotting analysis shows the effects of knocking down the Akt, NF-κB, β-catenin or EZH2 genes in combination with TClC and L-theanine (T) on the protein expression of CD133, CD44, ALDH1, ABCG2, EGF, HGF, VEGF and OPN in A549 **(E)** and LLC **(F)** cells. TClC enhanced the inhibitory effects of single knockdowns on protein expression in A549 and LLC cells, as indicated by the stronger inhibitory effects of TClC than that of L-theanine (T). GAPDH served as a loading control.

efficacy of TClC in suppressing migration and invasion (Fig. 6A and B). The representative results of the cell invasion assays are shown in Fig. 6C and D for A549 and LLC cells. These data suggest that the multitarget mechanism of TClC compensates for the absence of a single molecule. Importantly, TClC consistently had stronger inhibitory effects on the growth, migration, and invasion of LLC and A549 cells than did L-theanine.

In addition, we confirmed that knockdown of AKT, NF-κB, β-catenin, or EZH2 alone led to upregulation of E-cadherin protein expression and significant downregulation of EGF, HGF, VEGF, and OPN protein expression, in addition to affecting the protein levels of AKT, NF-κB, β-catenin, and EZH2 in both A549 (Fig. 6E and Fig. S6A-D) and LLC cells (Fig. 6F and Fig. S6E-H). Knockdown of AKT, NF-κB, β-catenin, or EZH2 resulted in a greater than 50 % decrease in the protein levels of EGF, HGF, VEGF and OPN, as shown in Fig. 6E and F. TClC had similar effects, inducing decreases in the expression of EGF, HGF, VEGF, and OPN, as well as increases in E-cadherin expression in LLC and A549 cells (Fig. 6E and F), indicating that TClC had much stronger effects than L-theanine on protein expression.

Moreover, we demonstrated that the knockdown of AKT, NF-κB, β-catenin, or EZH2 alone also resulted in downregulation of the protein expression of lung cancer stem cell markers as well as the drug resistance-related proteins CD133, CD44, ALDH1 and ABCG2 in NSCLC A549 and LLC cells. TClC also had protein-suppressive effects, leading to the downregulation of CD133, CD44, ALDH1 and ABCG2 protein expression in A549 cells (Fig. 6E) and LLC cells (Fig. 6F), revealing that

the effect of TClC was much greater than that of L-theanine on protein expression. Collectively, these data suggest that the functional loss of AKT, NF-κB, β-catenin, or EZH2 hinders cell migration and invasion, similar to the inhibitory effect of TClC on these cellular processes. In addition, knockdown of AKT, NF-κB, β-catenin or EZH2, or TClC treatment resulted in significant decreases in the expression of the tumor-secreted factors EGF, HGF, VEGF, and OPN; cancer stem cell markers; and the drug resistance-related proteins CD133, CD44, ALDH1 and ABCG2 in NSCLC cells.

3. Discussion

In this study, we discovered a new promising anticancer polypharmacological agent for treating NSCLC. First, we developed a novel semisynthesized bioactive compound called ethyl 6-chlorocoumarin-3-carboxylyl L-theanine (TClC) by combining the beneficial properties of L-theanine and coumarin. We show that TClC has a markedly greater antitumor effect than its parent compound L-theanine in eliminating NSCLC cells and inhibiting the invasion and metastasis of NSCLC both *in vitro* and *in vivo*. Notably, TClC stands out from the clinical cancer drugs cisplatin, gefitinib, gemcitabine and pirarubicin in NSCLC cells. Compared with clinical drugs, TClC suppresses tumor growth and metastasis in mice as a monotherapy with greater efficacy and sensitizes tumors to cancer drugs such as gefitinib and cisplatin via combination treatment *in vivo*. In addition, we demonstrated the unique mechanism of action of TClC by identifying multiple cancer effectors, including AKT, β-catenin, EZH2, NF-κB, and PD-L1, as molecular targets in NSCLC. In an attempt to investigate the CD133+ stem-like NSCLC population, we reveal that TClC inhibits cell viability, EMT, migration and invasion in this tumor subset and reduces the expression of a set of oncogenic factors and EMT transcription factors, accompanied by decreases in TNF-α-induced NF-κB activity and the activities of MMP9 and MMP2 and, importantly, the suppression of PD-L1 expression. Subsequent target gene knockdown studies further confirmed that the effects of TClC treatment on NSCLC cells are comparable to the knockdown effects of its targets. Overall, this study reports a new promising polypharmacological anticancer agent TClC for the treatment of NSCLC.

A major advantage of TClC is that it exhibited low toxicity in our experimental models, which is of paramount importance when considering its potential clinical utility. Compared with L-theanine and coumarin, TClC had a significantly longer half-life (approximately 6 h) (Fig. 1). This extended half-life is crucial for ensuring sustained therapeutic efficacy and reducing the frequency of dosing [23], which can enhance patient compliance and convenience. Importantly, TClC exhibited remarkable efficacy in inhibiting the growth and metastasis of NSCLC *in vivo* via both monotherapy and combination therapy with clinical drugs. Our results demonstrated that TClC outperformed L-theanine in terms of its ability to suppress tumor progression. These characteristics highlight the potential of TClC as a promising candidate for NSCLC treatment, which may lead to improved therapeutic outcomes. Additionally, we demonstrated the strong anticancer effects of TClC, its potential to inhibit stem-like traits, its potential ability to overcome drug resistance, and its ability to prevent metastasis. Crucially, TClC achieves these benefits without harming healthy cells. *In vitro*, TClC selectively targeted tumor cells without affecting normal cells. *In vivo*, TClC had no significant effect on body weight in these mice. These findings underscore the potential clinical applicability of TClC. More importantly, TCIC predominantly accumulates in tumor tissues with minimal presence in vital organs such as the liver, spleen, heart, lungs, and kidneys, as shown in Figs. S2E and S2F. Moreover, TCIC has negligible effects on the hERG ion channel, which is essential for cardiac safety (Fig. S7).

Given the genetic heterogeneity and complex signaling pathways involved in NSCLC, a multifaceted approach is necessary, as single-molecule targeting has limited efficacy [65–67] and adaptive resistance sometimes mitigates the effects of KRAS inhibitors [68]. Polypharmacological strategies against cancer cells have shown promise in reducing the risk of resistance to single-target inhibitors and improving patient survival [69]. We found that TClC exhibits a polypharmacological effect that is crucial for overcoming the intricate network of compensatory pathways in NSCLC [70–72]. Further exploration is necessary to delineate the interactions among key regulatory genes and factors upstream of critical pathways such as AKT, NF-κB, β-catenin, EZH2, and PD-L1. By integrating polypharmacology with network pharmacology, we could deepen our understanding of NSCLC's molecular pharmacology and pathology, paving the way for novel therapeutic insights.

In our molecular studies, TClC was subjected to extensive analysis including molecular docking and molecular dynamics simulations, revealing its affinity for key proteins such as EZH2, AKT1, AKT2, NF-κB, PD-L1, and β-catenin. Subsequent validation efforts using techniques like DARTS, TSA, and SPR, coupled with functional assays, confirmed these targets. Detailed docking studies showed that TClC interacts with crucial functional domains of these proteins through specific residues—Lys, Tyr, Arg, and Asp—illustrating a complex interaction landscape (Tables S1–2, Fig. 5B). For instance, in EZH2, the coumarin group of TClC was inserted into a cavity containing Tyr111, Tyr658 and Tyr661, destroying the van der Waals interaction between Tyr111 and Tyr661 [59]. TClC also exhibited hydrophobic interactions with key tryosines in PD-L1, NF-κB and AKTs, and these interactions resembled those of positive inhibitors of the corresponding targets. In addition, Cys663 is considered a substrate residue for affording SAM noncompetitive EZH2 inhibitors [73], and the branched groups of TClC are located in the hydrophobic region formed by Cys663, Phe665 and Met662. For AKT1 and AKT2, TClC is involved in hydrogen bonding interactions with key lysines (Lys 158 for AKT1 and Lys181 for AKT2) in the P-loop, inhibiting the activities of the kinases [74,75]. For β-catenin, TClC is inserted in the hydrophobic cleft lined by the residues Cys466 and Pro463 of β-catenin, affecting the transcriptional activity of β-catenin [76] and interaction with the TCF-4 transcription factor [77]. Arg469 is a key amino acid involved in the interaction between β-catenin and TCF4 [77], and TClC forms hydrophobic contacts with Arg469 to affect this interaction. For NF-κB, TClC forms one bifurcated H-bond with Lys218 and multiple hydrophobic bonds with Arg187, Ala188 and Asp217. For PD-L1, Tyr56 and Met115 are known to be binding sites for BMS inhibitors, such as BMS-202, interrupting PD-L1/PD-1 complex binding [78]. TClC interacts with these amino acid residues, indicating the potential disruption of complex formation in NSCLC. Although further investigations of these binding sites by using methods such as mutagenesis approaches (site-directed mutagenesis or random-and-extensive mutagenesis) may provide deeper insight into the specific binding modes of TClC to its target, the polypharmacological effect of TClC revealed in this study could be advantageous in cancer therapy, as it allows simultaneous modulation of several pathways involved in tumor growth, therapeutic resistance and metastasis.

Considering that the enrichment of stem-like cancer cells is one of the major causes of drug resistance, tumor progression and metastasis, we investigated the role of CD133+ LC cells in NSCLC tumors and the efficacy of TClC against these cells. CD133+ LC and A549 cells secreted elevated levels of oncogenic factors, including HGF, EGF, OPN [79], VEGF, and MMP9 [80], which contributed to tumor cell growth and progression (Fig. 4 and Table 1). The media derived from cultured CD133+ LC cells, along with EGF and HGF, significantly enhanced the viability, growth, EMT, migration, and invasion of CD133+ LC and A549 cells, suggesting that the tumor-secreted factors might stimulate mesenchymal phenotypic changes in NSCLC cells and increase their aggressiveness, forming an autocrine feedback loop. These effects are likely mediated by the PI3K/Akt, NF-κB, β-catenin, EZH2, and PD-L1 signaling pathways, which can be suppressed by TClC and pathway inhibitors. Recent studies have emphasized the critical roles of elevated EZH2 and key signaling pathways, such as the WNT/TCF [81], NF-κB [82], and PI3K/AKT/mTOR pathways [83], in NSCLC progression and

metastasis. The crosstalk among AKT, NF-κB, β-catenin, and EZH2 in NSCLC is evident from the effects observed upon their knockdown or treatment with inhibitors in A549 and LLC cells. The effectiveness of TCIC stems from its multi-target approach, which affects the Akt, NF-κB, β-catenin pathways, as well as the epigenetic pathway EZH2 and the anti-tumor immune target PD-L1. This multi-target action enables TCIC to effectively inhibit the growth and metastasis of lung cancer, which is notoriously difficult to treat. Our findings suggest that instead of combination therapy with multiple drugs, the ability of TClC to safely target multiple oncogenic proteins has important clinical implications.

Our study establishes a robust foundation for advancing TClC research, highlighting the necessity of assessing its efficacy and safety as a precursor to clinical trials. Future efforts should concentrate on optimizing pharmaceutical formulations and devising treatment strategies that include tumor-specific TClC delivery methods and combinations with other chemotherapeutic drugs. This research is particularly relevant for the treatment of lung cancer and other aggressive cancers such as metastatic breast cancer, brain tumors, and melanoma. These cancers express high levels of TClC target proteins, and preliminary data suggest that TClC significantly inhibits metastasis and invasion in these contexts. Additionally, comprehensive pharmacokinetic and toxicological studies across various animal models are essential to facilitate clinical trial readiness.

In conclusion, our study emphasizes the therapeutic potential of TClC, a semi-synthesized bioactive compound utilized as a polypharmacological agent, underscoring the importance of polypharmacological treatment strategies in managing refractory or metastatic NSCLC. By effectively targeting multiple key oncogenic proteins and suppressing the pro-tumorigenic, EMT, migration, invasion, and metastatic activity of CD133+ LC cells, TClC offers a promising approach for curbing the progression and spread of NSCLC. These results contribute to the development of new strategies for drug discovery and innovative lung cancer therapies and provide crucial insights into the mechanisms driving NSCLC progression and metastasis. The utilization of TClC polypharmacology, which involves the concurrent targeting of multiple critical proteins, shows promise as an effective approach for combating NSCLC.

4. Materials and methods

4.1. Chemicals and antibodies

Primary antibodies against E-cadherin, β-catenin, CD133, CD44, ALDH1, ABCG2, NF-κB, EZH2, N-cadherin, vimentin, snail-1, slug, ZEB, twist, histone-3, Bax, Bcl-2, and GAPDH were purchased from Santa Cruz Technology Inc. (Shanghai, China). Primary antibodies against EGF, EGFR, HGF, OPN, VEGF, and AKT were obtained from Cell Signaling Technology, Inc. (Beverley, MA, USA). ELISA kits for EGF, HGF, VEGF, OPN, MMP9, INF-γ, and TNF-α and CSC medium were purchased from R&D Systems, Inc. (Shanghai, China). Fibronectin and Boyden chambers were obtained from BD Inc. (BD Biosciences, San Jose, CA, USA) and Corning, Inc. (Corning, NY, USA), respectively. Gemcitabine, gefitinib, cisplatin, and pirarubicin were purchased from Yantai Yuhuangding Hospital, China. DMEM, RPMI 1640 medium, penicillin, streptomycin, fetal bovine serum (FBS), trypsin/EDTA, propidium iodide (PI), 3-[4,5-dimethylthiazol-2-yl]-2,5-diphenyltetrazolium bromide (MTT), EPZ 6438 (tazemetostat, an inhibitor of EZH2), IWP-2, LY294002 (Ly), Bay 11–7082 (Bay), DMSO, the primary antibody for PD-L1 and all other chemicals, including materials for the synthesis of TClC, were acquired from Sigma-Aldrich (Shanghai, China).

4.2. Synthesis of ethyl 6-chlorocoumarin-3-carboxylyl L-theanine (TClC)

6-Chloro-2-oxo-2H-chromene-3-carboxylic acid (ClC) was obtained according to previous methods [84]. The products of all the reactions were monitored via thin-layer chromatography on 0.25 mm silica gel plates (60 GF-254) and visualized with UV light or ninhydrin spray (0.5 % in butanol). Melting points were determined on an electrothermal melting point apparatus.

TClC synthesis: $SOCl_2$ (0.055 mL, 0.76 mM) was slowly added to a solution of L-theanine (87 mg, 0. 5 mM) in absolute ethanol (1 mL). The mixture was stirred at room temperature for 2 h. Then, the resulting mixture was concentrated under reduced pressure to give ethyl *L*-theanine (ET). After CH_2Cl_2 (20 mL) was added to the obtained oily residue ET, 6-choloro-2-oxo-2H-chromene-3-carboxylic acid (ClC) (224 mg, 1 mM), 1.07 mL of DIPEA (0.7918 g, 0.61 mM), and 383 mg of EDCI (0.2 M) were added. The mixture was then stirred at room temperature for 1 h and concentrated under reduced pressure to remove the solvent. The crude product was purified by chromatography (acetone/petroleum ether = 1/5) on silica gel (yield = 76.6 %; purity = 98.2 %). m.p.: 118–120 °C. ^{1}H and ^{13}C NMR spectra were obtained on a Bruker Avance 500/125 spectrometer using tetramethylsilane (TMS) as an internal standard in DMSO-d_6 or $CDCl_3$ solutions. Chemical shifts were reported in delta (δ) units, parts per million (ppm) downfield from trimethylsilane. HRMS data were acquired using a Q Exactive™ Orbitrap MS system (Thermo Scientific, Waltham, MA, USA) equipped with a heated electrospray ionization (HESI) source. ^{1}H NMR (500 MHz, $CDCl_3$) δ 1.12 (t, J = 7.25 Hz, 3H, CH_3), 1.28 (t, J = 7.2 Hz, 3H, CH_3), 2.15–2.40 (m, 4H, CH_2), 3.26 (m, 2H, NH-CH_2), 4.14 (m, 1H, NH-CH), 4.21 (q, J = 7.1 Hz, 2H, O-CH_2), 5.47 (br, 1H, NH), 6.91 (d, J = 8.6 Hz, 1H, coumarin-8H), 7.25–7.28 (m, 2H, coumarin-5H,7H), 8.33 (s, coumarin-4H), 12.93 (s, 1H, NH). ^{13}C NMR δ: 14.1 (CH_3), 14.8 (CH_3), 29.1 (CH_2), 32.0 (CH_2), 34.4 (CH_2), 61.6 (CH), 70.0 (CH_2), 118.7 (C), 119.3 (CH), 123.4 (C), 130.9 (CH), 132.7 (CH), 159.6 (C), 166.3 (C), 170.7 (C), 171.2 (C). HRMS (*m/z*): 409.1141 $[M+H]^+$.

4.3. Detection of in vitro and in vivo fluorescent signals

TClC (80 mg/kg) or DMSO was intraperitoneally (i.p.) injected into C57BL/6 mice. Three hours later, *in vivo* or *in vitro* fluorescence images (TClC at 8 mg/mL in a tube) were recorded under 530 nm excitation and 595 nm emission. For *in vivo* or *ex vivo* fluorescence imaging in BALB/c *nu/nu* mice, 5×10^6 A549 cells suspended in 0.1 mL of Hank's balanced salt solution were intravenously (i.v.) injected into the rear flank of each BALB/c *nu/nu* mouse. Twelve days later, TClC (80 mg/kg) or L-theanine (80 mg/kg) was administered via intravenous injection into the tail vein of BALB/c *nu/nu* mice. Subsequently, *in vivo* or *ex vivo* fluorescence images (post-dissection of the liver, spleen, heart, lungs, kidneys, and tumor) were captured using a 530 nm excitation wavelength and 595 nm emission wavelength. The images were obtained on a Kodak Image Station 4000 Multi-Modal Imaging System (IS4000MM) instrument equipped with an X-ray unit and on a Kodak Image Station 2000 (Carestream Health, Rochester, NY, USA).

4.4. Preparation of sera from TClC-treated rats for ex vivo serum pharmacology analysis

The sera were prepared according to our previously published methods [44,46]. Briefly, Sprague-Dawley (SD) rats (age range, 6 weeks; Beijing Vital River Laboratory Animal Technology Co., Ltd., Beijing, China) were treated in accordance with guidelines established by the Institutional Animal Care and Use Committee at Yantai University (IACUC), China, and were approved by the IACUC of Yantai University. TClC or L-theanine was orally administered to the rats once daily at a dose of 80 mg/mL/kg body weight. Blood was then collected at 0, 0.5, 1, 3, 5, and 8 h from the rats (fasted for 16 h) after oral intubation. The collected blood was left to clot for 2 h at room temperature and subsequently centrifuged twice at 3000 × *g* at 4 °C for 20 min. The serum samples were sterilized by filtration and then heated at 56 °C for 30 min. Then, the A549 cells were grown in DMEM supplemented with rat serum at a concentration of 10 %, and cell growth was measured using the MTT assay.

4.5. Cell culture and in vitro growth assay

A549, NCI-H460 (H460), MRC-5, highly metastatic murine Lewis lung carcinoma (LLC), and melanoma B16F10 cell lines were obtained from the American Type Culture Collection. A549, H460, LLC, MRC-5, and B16F10 cells were cultured in DMEM, and human peripheral blood lymphocytes (PBLs) were cultured in RPMI 1640 medium supplemented with 10 % fetal bovine serum (FBS), glutamine (2 mM), penicillin (100 U/mL) and streptomycin (100 μg/mL). The cells were seeded in 96-well plates at 2×10^3 per well (1×10^5 per well for the case of PBL) and incubated overnight. The cells in the control group were treated with 0.1 % (v/v) DMSO. The cells were incubated in complete medium containing different concentrations of TClC or L-theanine (T, 16–250 μM), tazemetostat (EPZ, 125 μM), IWP-2 (10 μM), LY294002 (Ly, 25 μM), Bay (3.2 μM), or a combination of existing anticancer drugs (gemcitabine at 16–32 μM, gefitinib at 16–32 μM, cisplatin at 16–32 μM and pirarubicin at 16–32 nM). After 48 and 72 h of treatment, the absorbance values in each test group were measured using the MTT assay. Human PBLs were separated according to a previously reported method [42]. CD133+ LC cells were isolated from A549 cells and identified by fluorescence-activated cell sorting (FACS) for use as a marker of CSCs as well as for their sphere-forming capacity and other CSC characteristics. CD133+ LC cells were cultured in CSC medium and treated with TClC and L-theanine at concentrations ranging from 16 to 250 μM. After 4 days of treatment, the viability of the cells in each test group was measured using the Trypan blue exclusion test (TBET) (for 6-well plates) and MTT (for 96-well plates). In the case of CSCM-, or EGF plus HGF-treated cells, A549 cells (3.5×10^5 per well in 6-well plates) were treated with TClC and L-theanine for 30 min. Then, the cells were treated with EGF (60 μg/mL) plus HGF (100 μg/mL) or INF-γ (20 ng/mL) for 24 h, 48 h or longer.

4.6. Migration and invasion assays

Tumor cell migration and invasion were measured by modified Transwell chambers coated with fibronectin (for migration) and Matrigel™ (for invasion) or without fibronectin and Matrigel™ (Corning) [43,46]. In brief, cells (5×10^4) were seeded in the upper chamber in 200 μL of serum-free medium containing different concentrations of TClC or L-theanine (T, 16–125 μM), tazemetostat (EPZ, 125 μM), IWP-2 (10 μM), LY294002 (Ly, 25 μM), or BAY 11-7082 (Bay, 3.2 μM); the lower compartment was filled with 660 μL of DMEM supplemented with 10 % FBS in the presence or absence of an equal volume of the supernatant from 48 h-/96 h-CD133+ LCs (CSCM, 48 h/96 h) or EGF (60 μg/mL) plus HGF (100 μg/mL). After incubation for 6 h (for migration) or 20 h (for invasion), the cells on the lower surface of the filter were fixed and stained with propidium iodide. The cells on the upper side of the filter were removed using a rubber scraper. The cells on the lower side of the membrane were counted and recorded under a fluorescence microscope (Nikon, TE2000-U, Japan).

4.7. Subcutaneous (s.c.) and metastatic tumor xenograft models

Female BALB/c *nu/nu* mice and C57BL/6 mice (age range, 6 weeks) were purchased from Beijing Vital River Laboratory Animal Technology Co., Ltd. (Beijing, China). Single-cell suspensions containing 1.6×10^6 A549 cells or 0.5×10^6 LLC cells in 0.1 mL Hank's balanced salt solution were injected s.c. into the rear right flank of each BALB/c *nu/nu* mouse (in the case of A549 cells) or each C57BL/6 mouse (in the case of LLC cells). After 10–15 days, the tumor-bearing mice were randomly divided into 4 groups (6 or 7 mice per group): (1) the control group (vehicle), (2) the cisplatin group (1.5 mg/kg/i.p./d), (3) the L-theanine group (80 mg/kg/i.p./d), and (4) the TClC group (80 mg/kg/i.v./d). The mice were treated by intraperitoneal (i.p.) or intravenous (i.v.) injection of drugs. Treatment was administered for 16 days (for the case of LLC tumors) or 28 days (for the case of A549 tumors). Tumor measurements and volume calculations were performed according to methods described in earlier studies [85–87]. On the study endpoint day, the mice in all the groups were sacrificed. For the lung cancer metastasis model, single-cell suspensions containing 5×10^5 LLC cells in 0.1 mL Hank's balanced salt solution were injected into the tail vein of each C57BL/6 mouse, and 27 days of drug treatment were administered on the following days. The experimental mice were randomly divided into 7 groups (6 mice per group): (1) the control group (vehicle), (2) the cisplatin (DDP) group (1.5 mg/kg/i.p./d), (3) the gefitinib (Gef) group (250 mg/kg/p.o./d), (4) the L-theanine (T) group (80 mg/kg/i.p./d), (5) the TClC group (80 mg/kg/i.v./d), (6) the DDP + TClC group (DDP 1.5 mg/kg/i.p./2 d + TClC 40 mg/kg/i.v./d), and (7) the Gef + TClC group (Gef 250 mg/kg/p.o./2 d + TClC 40 mg/kg/i.v./d). On the 28th day, the mice in all the groups were sacrificed. The number of metastatic nodules, including large (diameter ≥3 mm) and small (diameter <3 mm) nodules, in the lung was recorded. The lungs were fixed in Bouin's solution, destained in 70 % ethanol, and examined for the number of lung metastatic nodules under a light microscope. LLC metastatic nodules were compared among the groups using ANOVA and the Bonferroni correction. The values are shown as the mean ± SEM (n = 6–7) for each group.

4.8. ELISA detection of the protein levels of HGF, EGF, VEGF, OPN, and/or MMP9 in the supernatants of cancer cells

Equal amounts of the supernatants of A549 and CD133+ LC cells were analyzed via ELISA using kits for HGF, EGF, VEGF, OPN and/or MMP9 from R&D Systems, Inc. (Shanghai, China), according to the manufacturer's instructions.

4.9. Gelatin zymography

The serum samples of the supernatants (serum-free) from the upper chamber of the Transwell chamber in the aforementioned serum-free invasion assay were analyzed for MMP9/MMP2 activation. The samples were subjected to 10 % SDS-PAGE containing 0.1 % gelatin under nonreducing conditions. Following electrophoresis, the gels were washed with 2.5 % Triton X-100 and then incubated in developing buffer [50 mM Tris-HCl buffer (pH 7.4), 10 mM $CaCl_2$] overnight at 37 °C. The gels were stained with 0.25 % Coomassie Brilliant Blue R-250 and destained in the same solution without dye. Gelatinase (MMP) activation was visualized as clear bands against the blue-stained gelatin background.

4.10. Molecular docking

The Surflex-Dock program in Sybyl-X 2.1.1 software (Tripos, Inc., St. Louis, MO, USA) was used to identify possible binding modes of TClC and its six tumor targets (EZH2, AKT1, AKT2, NF-κB, β-catenin, and PD-L1). The 3D structure of TClC was generated and optimized using the Tripos force field and Gasteiger-Huckel charges via the minimize module. The 3D structures of EZH2 (PDB ID: 5IJ7) [59], PD-L1 (PDB ID: 5N2F) [88], AKT1 (PDB ID: 4GV1) [74], AKT2 (PDB ID: 2X39) [89], and β-catenin (PDB ID: 7AR4) [90] were used for docking, and the active sites were defined as the binding pockets of the ligands in the crystal structures. Since there is no complex of NF-κB and its inhibitor, the active site in this target (PDB: 3GUT) [91] was defined based on the verified contact residues Arg33, Arg35, Tyr36, Arg187 and Gln220 from Mulakayala et al.'s work [92]. The default settings for ligand-protein docking were used throughout the simulations. The 2D plots were generated using LIGPLOT v2.2.4 [93].

4.11. Molecular dynamics (MD) simulation

To investigate the stable states of ligand-protein binding interactions, six independent simulations were carried out for TClC interacting with six tumor targets. The initial coordinates of TClC in the

proteins were derived from the abovementioned docking conformations, and the simulations were performed with GROMACS 5.1.4 [94]. Taking the TClC-EZH2 simulation as an example, the protein was first modeled with AMBER99SB-ILDN [95] and a GAFF force field was applied for TClC using the program antechamber in AMBER14 [96]. The system was dissolved with TIP3P waters, and the charges were neutralized with 0.15 M NaCl. Then, energy minimization was carried out for the system using the steep-descent algorithm for 50000 steps. The canonical ensemble was performed by heating the system from 0 K to 300 K via velocity rescaling [97], and the isothermal-isobaric ensemble (P = 1 bar and T = 300 K) was constructed by means of the Parrinello-Rahman barostat [98,99] for 100 ps. Finally, a 100 ns production run was performed for the ligand-protein complex. The root-mean-square deviation (RMSD) calculated from the MD trajectory was used to verify the stability of the ligand-protein complex. Moreover, a cluster protocol based on the RMSD of the conformations determined using the GROMOS clustering algorithm [100] was used to extract the representative conformation from the dynamically equilibrated MD trajectory.

4.12. Drug affinity responsive target stability (DARTS) assay

DARTS experiments were performed according to previously reported methods and previous publications including ours [61–63]. In brief, cells were washed with cold PBS and then lysed with a protein extraction kit (Beyotime, Haimen, China). After centrifugation (14,000 rpm for 15 min), the lysates were mixed with 10 × TNC buffer (0.5 M NaCl, 0.1 M $CaCl_2$, 0.5 M Tris/HCl pH 8.0). Then, the lysates (1 × TNC buffer) were incubated with DMSO or TClC for 30 min at room temperature after they had incubated for 60 min at 4 °C. After incubation, each sample was proteolyzed with 0 or 0.1 % pronase for 15 min at room temperature. To stop proteolysis, 2 μL of ice-cold buffer containing 20 × protease inhibitor cocktail was added. An equal amount of each treated sample was loaded onto SDS-PAGE gels for Coomassie blue staining or Western blotting.

4.13. Western blot analysis

According to our previously described methods [42,44], the cells were treated with different concentrations of TClC. The treated cells were collected at 48 h. Total cellular proteins were extracted, and the cytosolic fractions and nuclear proteins were prepared following the procedure described by the Nuclear and Cytoplasmic Protein Extraction Kit (P0028, Beyotime, Biotechnology, Inc., Shanghai, China). The protein concentration of the extracts was determined using the Bradford method. Equal amounts of cell extracts were resolved by SDS-PAGE, transferred to nitrocellulose membranes, and probed with primary antibodies against the detected proteins and then with horseradish peroxidase-conjugated secondary antibodies. Detection was performed using an enhanced chemiluminescence system (GE Healthcare Life Sciences, Piscataway, NJ, USA). The intensity of protein expression was quantified using ImageJ and is shown as values, normalized to those of the internal control (e.g., GAPDH) and the corresponding control (e.g., shRNA control), ranging from 0 to 1 under the corresponding bands.

4.14. Transfection of short hairpin RNAs (shRNAs) targeting EZH2, β-catenin, AKT, or NF-κB p65

A549 and LLC cells were transfected with the EZH2 (ENX-1) shRNA plasmid, the β-catenin shRNA plasmid, the AKT shRNA plasmid, the NF-κB p65 shRNA plasmid and the scrambled nontargeting shRNA control (Santa Cruz Technology Inc., Shanghai, China) using Lipofectamine transfection reagent according to the manufacturer's instructions and our reported methods [42,44].

4.15. Statistical analysis

The data are expressed as the mean ± standard deviation (S.D.) and were analyzed by SPSS 16.0 software to determine significant differences. Statistical analysis was performed using ANOVA and the Bonferroni post hoc test. The values between the different treatment groups at different times were compared. The relative cell growth, migration and invasion rates; normalized NF-κB p65 activity; relative protein levels; relative tumor volumes; relative tumor weights; and lung cancer metastasis status are shown for each group. Unless otherwise specified, values are presented as the mean ± SEM for each group, with n = 3 biological replicates. For the tumor growth and metastasis experiments, where the values represent the mean ± SEM for each group (n = 6–7). For all tests, *p* values less than 0.05 were considered to indicate statistical significance. All the statistical tests were two-sided.

CRediT authorship contribution statement

Jing Lu: Writing – review & editing, Writing – original draft, Visualization, Investigation, Formal analysis, Data curation. **Ying Zhang:** Writing – review & editing, Writing – original draft, Visualization, Investigation, Formal analysis, Data curation. **Chunyan Yan:** Writing – original draft, Visualization, Investigation, Formal analysis, Data curation. **Jingwen Liu:** Writing – original draft, Investigation, Formal analysis, Data curation. **Dan Qi:** Writing – review & editing, Writing – original draft, Visualization, Investigation, Formal analysis, Data curation. **Yue Zhou:** Writing – original draft, Investigation, Data curation. **Qinwen Wang:** Writing – original draft, Investigation, Formal analysis. **Juechen Yang:** Writing – original draft, Investigation, Formal analysis. **Jing Jiang:** Writing – original draft, Investigation, Formal analysis. **Benhao Wu:** Writing – original draft, Visualization, Formal analysis. **Meiling Yang:** Writing – original draft, Visualization, Formal analysis. **Weiwei Zhang:** Data curation, Formal analysis, Writing – review & editing. **Xin Zhang:** Writing – original draft, Visualization, Formal analysis. **Xiaoyu Shi:** Writing – original draft, Visualization, Formal analysis. **Yan Zhang:** Writing – original draft, Visualization, Formal analysis. **Kun Liu:** Writing – original draft, Visualization, Formal analysis. **Yongcai Liang:** Writing – original draft, Visualization, Formal analysis. **Chaoyang Wang:** Writing – original draft, Visualization, Formal analysis. **Hanyu Yang:** Writing – original draft, Visualization, Formal analysis. **Yuqing Gao:** Writing – original draft, Visualization, Formal analysis. **Yuping Sun:** Writing – original draft, Visualization, Formal analysis. **Ronghu Ke:** Writing – review & editing, Writing – original draft, Visualization, Formal analysis. **Jason H. Huang:** Writing – review & editing, Supervision, Resources. **Min Wu:** Writing – review & editing, Supervision, Resources, Funding acquisition. **Hongbo Wang:** Writing – review & editing, Resources, Methodology. **Chunlei Li:** Writing – original draft, Resources, Investigation, Formal analysis. **Shuang Zhou:** Writing – original draft, Investigation, Formal analysis, Data curation. **Bin Guo:** Writing – review & editing, Supervision, Resources, Investigation, Conceptualization. **Erxi Wu:** Writing – review & editing, Writing – original draft, Supervision, Resources, Funding acquisition, Conceptualization. **Guoying Zhang:** Writing – review & editing, Writing – original draft, Supervision, Resources, Methodology, Funding acquisition, Conceptualization.

Data availability

Details on the synthesis of the new chemical entities described in this study are provided in the main text and supplemental information. All the experimental data generated or analyzed during this study are available from the corresponding authors upon reasonable request.

Ethical approval and consent to participate:

All animal experiments were performed with ethical approval from

the Institutional Animal Care and Use Committee (IACUC) of Yantai University (China).

No human subjects were involved in this study.

Declaration of competing interest

The authors declare the following personal relationships which may be considered as potential competing interests: Ying Zhang, Benhao Wu, Meiling Yang, Weiwei Zhang, Xin Zhang, Xiaoyu Shi and Yan Zhang are currently employed by Shandong Yingdong Yinghao Biotechnology Inc. Jing Jiang is currently employed by RemeGen, Ltd. Hanyu Yang, Yuqing Gao and Chunlei Li are currently employed by Shiyao Zhongqi Pharmaceutical Technology (Shijiazhuang) Co., LTD.

Acknowledgements

The study was partially supported by the National Key Research and Development Program of China (2017YFB0702600, 2017YFB0702602, 2017YFB0702602-2), the Shandong Provincial Natural Science Foundation (ZR2019MH076, ZR2022MH291), the Ministry of Science and Technology of the People's Republic of China ("863 grant", 2012AA020206), the Department of Science and Technology of Shandong Province (20092009GG10002087), the National Natural Science Foundation of China (81603024; 30973553), the NIH grant R01 CA186100, Wenzhou Institute University of Chinese Academy of Sciences, and Corbett Estate Fund for the Cancer Research (62285-531021-41800; 62285-531021-51800; 62285-531021-61800; 62285-531021-71800).

Appendix A. Supplementary data

Supplementary data to this article can be found online at https://doi.org/10.1016/j.bioactmat.2024.11.019.

References

[1] F. Bray, et al., Global cancer statistics 2022: GLOBOCAN estimates of incidence and mortality worldwide for 36 cancers in 185 countries, CA Cancer J Clin 74 (3) (2024) 229–263.
[2] The American Cancer Society medical and editorial content team, Key statistics for lung cancer, Lung Cancer (2024 Jan 29, 2024) [cited 2024 Jun 2024]; Available from: https://www.cancer.org/cancer/types/lung-cancer/about/key-statistics.html.
[3] R.L. Siegel, A.N. Giaquinto, A. Jemal, Cancer statistics, 2024, CA Cancer J Clin 74 (1) (2024) 12–49.
[4] C. Zappa, S.A. Mousa, Non-small cell lung cancer: current treatment and future advances, Transl. Lung Cancer Res. 5 (3) (2016) 288.
[5] R.S. Herbst, D. Morgensztern, C. Boshoff, The biology and management of non-small cell lung cancer, Nature 553 (7689) (2018) 446–454.
[6] Y. Tsukita, et al., Immunotherapy or Chemoimmunotherapy in Older Adults with advanced non-small cell lung cancer, JAMA Oncol. 10 (4) (2024) 439–447.
[7] The American Cancer Society medical and editorial content team, Lung cancer survival rates, Lung Cancer (2024 January 29, 2024) [cited 2024 Jun 2024]; Available from: https://www.cancer.org/cancer/types/lung-cancer/detection-diagnosis-staging/survival-rates.html.
[8] A.K. Ganti, et al., Update of incidence, Prevalence, survival, and initial treatment in patients with non-small cell lung cancer in the US, JAMA Oncol. 7 (12) (2021) 1824–1832.
[9] A. Ashour Badawy, et al., Site of metastases as Prognostic factors in Unselected population of stage IV non-small cell lung cancer, Asian Pac. J. Cancer Prev. APJCP : Asian Pac. J. Cancer Prev. APJCP 19 (7) (2018) 1907–1910.
[10] V. Sosa Iglesias, et al., Drug resistance in non-small cell lung cancer: a potential for NOTCH targeting? Front. Oncol. 8 (2018) 267.
[11] K. Pan, et al., Emerging therapeutics and evolving assessment criteria for intracranial metastases in patients with oncogene-driven non-small-cell lung cancer, Nat. Rev. Clin. Oncol. 20 (10) (2023) 716–732.
[12] T.A. Martin, et al., Cancer invasion and metastasis: molecular and cellular perspective, in: Madame Curie Bioscience Database, Landes Bioscience, 2013 *[Internet]*.
[13] L. Li, et al., Expansion of cancer stem cell pool initiates lung cancer recurrence before angiogenesis, Proc Natl Acad Sci U S A 115 (38) (2018) E8948–E8957.
[14] G.L. Coles, et al., Unbiased Proteomic profiling Uncovers a targetable GNAS/PKA/PP2A Axis in small cell lung cancer stem cells, Cancer Cell 38 (1) (2020) 129–143, e7.
[15] G. Bertolini, et al., Highly tumorigenic lung cancer CD133+ cells display stem-like features and are spared by cisplatin treatment, Proc Natl Acad Sci U S A 106 (38) (2009) 16281–16286.
[16] H.E. Romeo, M.L. Barreiro Arcos, Clinical relevance of stem cells in lung cancer, World J Stem Cells 15 (6) (2023) 576–588.
[17] J. Li, et al., Trailblazing perspectives on targeting breast cancer stem cells, Pharmacol. Ther. 223 (2021) 107800.
[18] Y. Zheng, et al., Lung cancer stem cell markers as therapeutic targets: an Update on signaling pathways and therapies, Front. Oncol. 12 (2022) 873994.
[19] L. Wang, et al., Cisplatin-enriching cancer stem cells confer multidrug resistance in non-small cell lung cancer via enhancing TRIB1/HDAC activity, Cell Death Dis. 8 (4) (2017) e2746.
[20] A. Adini, et al., The stem cell marker prominin-1/CD133 interacts with vascular endothelial growth factor and potentiates its action, Angiogenesis 16 (2) (2013) 405–416.
[21] H. Peng, et al., Multiplex immunofluorescence and single-cell transcriptomic profiling reveal the spatial cell interaction networks in the non-small cell lung cancer microenvironment, Clin. Transl. Med. 13 (1) (2023) e1155.
[22] M.A. Socinski, et al., Treatment of stage IV non-small cell lung cancer: Diagnosis and management of lung cancer, in: third ed.*American College of Chest Physicians evidence-based Clinical Practice Guidelines.* Chest, vol. 143, 2013, pp. e341S–e368S, 5 Suppl.
[23] S.M. Liu, et al., Emerging evidence and treatment paradigm of non-small cell lung cancer, J. Hematol. Oncol. 16 (1) (2023) 40.
[24] PDQ® Adult Treatment Editorial Board, PDQ non-small cell lung cancer treatment, in: PDQ Cancer Information Summaries [Internet], 2024, 2024 Mar 8 [cited 2024 Jun 2024]; Available from: https://www.cancer.gov/types/lung/hp/non-small-cell-lung-treatment-pdq.
[25] The American Cancer Society medical and editorial content team, Treatment Choices for non-small cell lung cancer, by stage, Lung Cancer (2024 May 2, 2024) [cited 2024 Jun 2024]; Available from: https://www.cancer.org/cancer/types/lung-cancer/treating-non-small-cell/by-stage.html.
[26] D. Kim, et al., Pan-KRAS inhibitor disables oncogenic signalling and tumour growth, Nature 619 (7968) (2023) 160–166.
[27] D.S. Ettinger, et al., Non-small cell lung cancer, Version 3.2022, NCCN clinical Practice guidelines in Oncology, J Natl Compr Canc Netw 20 (5) (2022) 497–530.
[28] A. Olivares-Hernandez, et al., Immune checkpoint inhibitors in non-small cell lung cancer: from current perspectives to future treatments-a systematic review, Ann. Transl. Med. 11 (10) (2023) 354.
[29] J. Feng, et al., Safety and efficacy of immune checkpoint inhibitor rechallenge in advanced non-small cell lung cancer: a retrospective study, Sci. Rep. 14 (1) (2024) 2315.
[30] J. Mazieres, et al., Immune checkpoint inhibitors for patients with advanced lung cancer and oncogenic driver alterations: results from the IMMUNOTARGET registry, Ann. Oncol. 30 (8) (2019) 1321–1328.
[31] D.J. Propper, F.R. Balkwill, Harnessing cytokines and chemokines for cancer therapy, Nat. Rev. Clin. Oncol. 19 (4) (2022) 237–253.
[32] R.M. Bremnes, et al., The role of tumor stroma in cancer progression and prognosis: emphasis on carcinoma-associated fibroblasts and non-small cell lung cancer, J. Thorac. Oncol. 6 (1) (2011) 209–217.
[33] D. Frezzetti, et al., VEGF as a potential target in lung cancer, Expert Opin. Ther. Targets 21 (10) (2017) 959–966.
[34] R. Wang, et al., Tumor-associated macrophages provide a suitable microenvironment for non-small lung cancer invasion and progression, Lung Cancer 74 (2) (2011) 188–196.
[35] S. Brabletz, et al., Dynamic EMT: a multi-tool for tumor progression, EMBO J. 40 (18) (2021) e108647.
[36] S. Srivastava, et al., Chemokines and NSCLC: emerging role in prognosis, heterogeneity, and therapeutics, Semin. Cancer Biol. 86 (Pt 2) (2022) 233–246.
[37] T. Yu, et al., MetaLnc9 facilitates lung cancer metastasis via a PGK1-activated AKT/mTOR pathway, Cancer Res. 77 (21) (2017) 5782–5794.
[38] S. Yang, et al., FOXP3 promotes tumor growth and metastasis by activating Wnt/β-catenin signaling pathway and EMT in non-small cell lung cancer, Mol. Cancer 16 (1) (2017) 124.
[39] Z. Lu, et al., Long non-coding RNA NKILA inhibits migration and invasion of non-small cell lung cancer via NF-κB/Snail pathway, Journal of experimental & clinical cancer research 36 (1) (2017) 54.
[40] L. Bai, et al., Upregulation of SIRT6 predicts poor prognosis and promotes metastasis of non-small cell lung cancer via the ERK1/2/MMP9 pathway, Oncotarget 7 (26) (2016) 40377.
[41] T. Tsuchiya, et al., Oral administration of the amino acids cystine and theanine attenuates the adverse events of S-1 adjuvant chemotherapy in gastrointestinal cancer patients, Int. J. Clin. Oncol. 21 (6) (2016) 1085–1090.
[42] G. Zhang, et al., Inhibition of lung tumor growth by targeting EGFR/VEGFR-Akt/NF-kappaB pathways with novel theanine derivatives, Oncotarget 5 (18) (2014) 8528–8543.
[43] J. Liu, et al., Theanine from tea and its semi-synthetic derivative TBrC suppress human cervical cancer growth and migration by inhibiting EGFR/Met-Akt/NF-κB signaling, Eur. J. Pharmacol. 791 (2016) 297–307.
[44] G. Zhang, Y. Miura, K. Yagasaki, Inhibitory effects of theanine and sera from theanine-fed rats on receptor-mediated cancer cell invasion beneath mesothelial-cell monolayers, Cytotechnology 36 (1–3) (2001) 195–200.
[45] N. Bhattarai, et al., Anticancer potential of coumarin and its derivatives, Mini Rev. Med. Chem. 21 (19) (2021) 2996–3029.

[46] S. Wang, et al., Suppression of growth, migration and invasion of highly-metastatic human breast cancer cells by berbamine and its molecular mechanisms of action, Mol. Cancer 8 (2009) 81.
[47] G. Zhang, et al., Anti-cancer activities of tea epigallocatechin-3-gallate in breast cancer patients under radiotherapy, Curr. Mol. Med. 12 (2) (2012) 163–176.
[48] M.S. Al-Keilani, K.H. Alzoubi, S.A. Jaradat, The effect of combined treatment with sodium phenylbutyrate and cisplatin, erlotinib, or gefitinib on resistant NSCLC cells, Clin. Pharmacol. 10 (2018) 135–140.
[49] A. Li, et al., Gefitinib sensitization of cisplatin-resistant wild-type EGFR non-small cell lung cancer cells, J. Cancer Res. Clin. Oncol. 146 (7) (2020) 1737–1749.
[50] J. Lopez de Andres, et al., Cancer stem cell secretome in the tumor microenvironment: a key point for an effective personalized cancer treatment, J. Hematol. Oncol. 13 (1) (2020) 136.
[51] R. Suresh, et al., The role of cancer stem cells in recurrent and drug-resistant lung cancer, in: A. Ahmad, S.M. Gadgeel (Eds.), Lung Cancer and Personalized Medicine: Novel Therapies and Clinical Management, Springer International Publishing, Cham, 2016, pp. 57–74.
[52] Y. Kang, J. Massague, Epithelial-mesenchymal transitions: twist in development and metastasis, Cell 118 (3) (2004) 277–279.
[53] F. Du, et al., MRTF-A-NF-kappaB/p65 axis-mediated PDL1 transcription and expression contributes to immune evasion of non-small-cell lung cancer via TGF-beta, Exp. Mol. Med. 53 (9) (2021) 1366–1378.
[54] C.M. Blakely, et al., NF-kappaB-activating complex engaged in response to EGFR oncogene inhibition drives tumor cell survival and residual disease in lung cancer, Cell Rep. 11 (1) (2015) 98–110.
[55] E. Meylan, et al., Requirement for NF-kappaB signalling in a mouse model of lung adenocarcinoma, Nature 462 (7269) (2009) 104–107.
[56] L. Zhang, et al., Nuclear factor kappa B expression in non-small cell lung cancer, Biomed. Pharmacother. 167 (2023) 115459.
[57] M.S. Hayden, S. Ghosh, Regulation of NF-kappaB by TNF family cytokines, Semin. Immunol. 26 (3) (2014) 253–266.
[58] F. Weiss, D. Lauffenburger, P. Friedl, Towards targeting of shared mechanisms of cancer metastasis and therapy resistance, Nat. Rev. Cancer 22 (3) (2022) 157–173.
[59] A. Brooun, et al., Polycomb repressive complex 2 structure with inhibitor reveals a mechanism of activation and drug resistance, Nat. Commun. 7 (1) (2016) 1–12.
[60] S. Giridharan, M. Srinivasan, Mechanisms of NF-kappaB p65 and strategies for therapeutic manipulation, J. Inflamm. Res. 11 (2018) 407–419.
[61] F. Wang, et al., Nucleolin is a functional binding protein for salinomycin in neuroblastoma stem cells, J. Am. Chem. Soc. 141 (8) (2019) 3613–3622.
[62] B. Lomenick, et al., Target identification using drug affinity responsive target stability (DARTS), Proc. Natl. Acad. Sci. USA 106 (51) (2009) 21984–21989.
[63] B. Lomenick, et al., Target identification using drug affinity responsive target stability (DARTS), Current protocols in chemical biology 3 (4) (2011) 163–180.
[64] Y. Han, D. Liu, L. Li, PD-1/PD-L1 pathway: current researches in cancer, Am. J. Cancer Res. 10 (3) (2020) 727–742.
[65] T. Tozuka, et al., Poor efficacy of anti-programmed cell death-1/ligand 1 monotherapy for non-small cell lung cancer patients with active brain metastases, Thorac Cancer 11 (9) (2020) 2465–2472.
[66] N.M. Raghavendra, et al., Dual or multi-targeting inhibitors: the next generation anticancer agents, Eur. J. Med. Chem. 143 (2018) 1277–1300.
[67] C. Ceci, P.M. Lacal, G. Graziani, Antibody-drug conjugates: Resurgent anticancer agents with multi-targeted therapeutic potential, Pharmacol. Ther. 236 (2022) 108106.
[68] S.R. Punekar, et al., The current state of the art and future trends in RAS-targeted cancer therapies, Nat. Rev. Clin. Oncol. 19 (10) (2022) 637–655.
[69] E.B. Haura, et al., Phase I/II study of the Src inhibitor dasatinib in combination with erlotinib in advanced non–small-cell lung cancer, J. Clin. Oncol. 28 (8) (2010) 1387.
[70] A.C. Dar, et al., Chemical genetic discovery of targets and anti-targets for cancer polypharmacology, Nature 486 (7401) (2012) 80–84.
[71] A. Kabir, A. Muth, Polypharmacology: the science of multi-targeting molecules, Pharmacol. Res. 176 (2022) 106055.
[72] S. Klaeger, et al., The target landscape of clinical kinase drugs, Science 358 (6367) (2017).
[73] Y. Zhang, et al., Discovery of a new-generation S-Adenosylmethionine-Noncompetitive Covalent inhibitor targeting the lysine Methyltransferase enhancer of Zeste Homologue 2, J. Med. Chem. 66 (11) (2023) 7629–7644.
[74] M. Addie, et al., Discovery of 4-amino-N-[(1 S)-1-(4-chlorophenyl)-3-hydroxypropyl]-1-(7 H-pyrrolo [2, 3-d] pyrimidin-4-yl) piperidine-4-carboxamide (AZD5363), an orally Bioavailable, potent inhibitor of Akt kinases, J. Med. Chem. 56 (5) (2013) 2059–2073.
[75] I. Collins, Targeted small-molecule inhibitors of protein kinase B as anticancer agents, Anti Cancer Agents Med. Chem. 9 (1) (2009) 32–50.
[76] Y. Zhang, et al., Endothelial NO Synthase-dependent S-Nitrosylation of beta-catenin prevents its association with TCF4 and inhibits proliferation of endothelial cells stimulated by Wnt3a, Mol. Cell Biol. 37 (12) (2017).
[77] T.A. Graham, et al., Tcf4 can specifically recognize beta-catenin using alternative conformations, Nat. Struct. Biol. 8 (12) (2001) 1048–1052.
[78] C. Liu, N.P. Seeram, H. Ma, Small molecule inhibitors against PD-1/PD-L1 immune checkpoints and current methodologies for their development: a review, Cancer Cell Int. 21 (1) (2021) 239.
[79] S.I. Choi, et al., Osteopontin production by TM4SF4 signaling drives a positive feedback autocrine loop with the STAT3 pathway to maintain cancer stem cell-like properties in lung cancer cells, Oncotarget 8 (60) (2017) 101284–101297.
[80] C. Li, et al., FOXP3 facilitates the invasion and metastasis of non-small cell lung cancer cells through regulating VEGF, EMT and the Notch1/Hes1 pathway, Exp. Ther. Med. 22 (3) (2021) 958.
[81] D.X. Nguyen, et al., WNT/TCF signaling through LEF1 and HOXB9 mediates lung adenocarcinoma metastasis, Cell 138 (1) (2009) 51–62.
[82] S. Gu, et al., Danshen-honghua Ameliorates Stress-induced Menopausal Depression in rats, Neural Plast. 2018 (2018) 6589608.
[83] H. Cheng, et al., Targeting the PI3K/AKT/mTOR pathway: potential for lung cancer treatment, Lung cancer management 3 (1) (2014) 67–75.
[84] M. Deshmukh, et al., A practical and environmentally friendly preparation of 3-carboxycoumarins, Synth. Commun. 33 (19) (2003) 3299–3303.
[85] A. Noel, et al., Basement membrane components (matrigel) promote the tumorigenicity of human breast adenocarcinoma MCF7 cells and provide an in vivo model to assess the responsiveness of cells to estrogen, Biochem. Pharmacol. 43 (6) (1992) 1263–1267.
[86] A.C. Noel, et al., Stromelysin-3 expression promotes tumor take in nude mice, J. Clin. Invest. 97 (8) (1996) 1924–1930.
[87] E. Wu, et al., Stromelysin-3 suppresses tumor cell apoptosis in a murine model, J. Cell. Biochem. 82 (4) (2001) 549–555.
[88] K. Guzik, et al., Small-molecule inhibitors of the programmed cell death-1/programmed death-ligand 1 (PD-1/PD-L1) interaction via Transiently induced protein states and Dimerization of PD-L1, J. Med. Chem. 60 (13) (2017) 5857–5867.
[89] T. McHardy, et al., Discovery of 4-amino-1-(7 H-pyrrolo [2, 3-d] pyrimidin-4-yl) piperidine-4-carboxamides as selective, orally active inhibitors of protein kinase B (Akt), J. Med. Chem. 53 (5) (2010) 2239–2249.
[90] M. Wendt, et al., Bicyclic beta-Sheet Mimetics that target the transcriptional Coactivator beta-catenin and inhibit Wnt signaling, Angew Chem. Int. Ed. Engl. 60 (25) (2021) 13937–13944.
[91] J.C. Stroud, et al., Structural basis of HIV-1 activation by NF-kappaB–a higher-order complex of p50:RelA bound to the HIV-1 LTR, J. Mol. Biol. 393 (1) (2009) 98–112.
[92] C. Mulakayala, et al., Synthesis and evaluation of resveratrol derivatives as new chemical entities for cancer, J. Mol. Graph. Model. 41 (2013) 43–54.
[93] R.A. Laskowski, M.B. Swindells, LigPlot+: multiple ligand-protein interaction diagrams for drug discovery, J. Chem. Inf. Model. 51 (10) (2011) 2778–2786.
[94] M.J. Abraham, et al., GROMACS: high performance molecular simulations through multi-level parallelism from laptops to supercomputers, SoftwareX 1–2 (2015) 19–25.
[95] K. Lindorff-Larsen, et al., Improved side-chain torsion potentials for the Amber ff99SB protein force field, Proteins 78 (8) (2010) 1950–1958.
[96] D.A. Case, et al., AMBER 14, University of California, San Francisco, 2014.
[97] G. Bussi, D. Donadio, M. Parrinello, Canonical sampling through velocity rescaling, J. Chem. Phys. 126 (1) (2007) 014101.
[98] M. Parrinello, A. Rahman, Polymorphic transitions in single crystals: a new molecular dynamics method, J. Appl. Phys. 52 (12) (1981) 7182–7190.
[99] S. Nosé, M.L. Klein, Constant pressure molecular dynamics for molecular systems, Mol. Phys. 50 (5) (1983) 1055–1076.
[100] X. Daura, et al., Peptide folding: when simulation Meets experiment, Angew. Chem. Int. Ed. 38 (1–2) (1999) 236–240.